ELECTRONIC DESIGN AUTOMATION

TECHNISCHE UNIVERSITÄT MÜNCHEN

Research Internship

Enhancing Signal Quality in Wavelength-Routed Optical Ring Networks-on-Chip via Simulation-Guided Power Compensation and Wavelength Configuration

Maximilian Häringer

ELECTRONIC DESIGN AUTOMATION

TECHNISCHE UNIVERSITÄT MÜNCHEN

Research Internship

Enhancing Signal Quality in Wavelength-Routed Optical Ring Networks-on-Chip via Simulation-Guided Power Compensation and Wavelength Configuration

Author:	Maximilian Häringer
Supervisor:	Zhidan Zheng
Submission Date:	13.05.2024

I confirm that this research internship is my own work and I have documented all sources and material used.

Munich, 13.05.2024 Maximilian Häringer

Abstract

Integrated circuits (ICs) have rapidly evolved over the past few decades, which has enabled multi-core and system-on-a-chip (SoC) architectures. Traditionally, electrical interconnects have been used for global on-chip communication, but their major drawbacks, such as capacitive and inductive coupling, a limited throughput and a high power consumption, have not been solved sufficiently. Because optical links circumvent the constraints imposed upon electronics, optical networks-on-chip (ONoCs) architectures based on photonic integrated circuits (PICs) emerge as a next-generation solution. Various types of ONoCs have been proposed, one of which is a wavelength-routed optical ring networks-on-chip (ORNoC) architecture. The performance of these ORNoCs needs to be simulated and evaluated in a practical environment.

In this work, a four-node ORNoC with full connectivity will be implemented, optimized and analyzed using the PIC simulator Ansys Lumerical INTERCONNECT. Based on a theoretical consideration, two feasible configurations - one having one waveguide, the other having two waveguides - are presented. Their component's properties are optimized and important performance factors listed for comparison. While the first configuration is characterized by seven wavelenghts, a total laser power of 272 mW, an average SNR of 17.28 dB and a maximum delay of 0.7 ns, the second configuration requires two wavelenghts, has a total laser power of 36 mW, an average SNR of 14.95 dB (15.23 dB) and a maximum delay of 0.4 ns.

Contents

1. Introduction

Ever since their invention, ICs have developed at a high speed following "Moore's Law". It states that the number of transistors on a microchip doubles approximately every two years, leading to an exponential increase in computing power [1]. As such, over the past decades, the semiconductor industry has revolutionized technology, enabling innovations such as the Internet of things, autonomous driving, and artificial intelligence.

Smaller transistors increase the transistor density which allows the integration of hundreds of cores on a single chip. Multi-core architectures enable parallel processing, which improves performance and efficiency [2]. However, system scaling enabled by Moore's scaling is more and more challenged with a lack of resources (e.g. in terms of power) and physical constraints [3]. As such, the semiconductor industry is expanding its research into further fields. In 2016, to provide a clear outline to simplify academic, manufacturing, supply, and research coordination regarding the development of electronic devices and systems, the "International Roadmap for devices and Systems" was launched [4]. It includes multiple international focus teams, one of which is "More Than Moore's Law". While following a roadmap based on Moore's Law ("More Moore") exclusively tries to scale down transistor sizes even further, "More Than Moore's Law" rather focuses on system integration and thus functional diversification with more functional components on a SoC [5].

Multi-core architectures and SoCs present challenges in designing efficient on-die interconnects. These interconnects should facilitate communication among numerous processor cores, memories, and specialized IP blocks on- and off-chip. Traditional interconnect methods like shared buses or global crossbars struggle to scale for large numbers of network endpoints, necessitating the development of efficient networks-on-chip (NoC) architectures to meet the communication demands of future many-core systems and SoCs [6].

Originally, electrical interconnects have been used for global on-chip communication. However, according to Le Beux et al. [7], they have a major drawback. Capacitive and inductive coupling enhance interconnect noise and propagation delay of global interconnects. Higher propagation delay requires global interconnects to operate with a lower clock frequency, which leads to lower upper bounds for achievable bandwidth and overall system performance. Various methods have been explored to improve

electrical interconnects, such as the insertion of repeaters into the RC line [8]. However, a limited throughput and a high power consumption are still known as dominant factors that restrict the scalability of electrical interconnects [9].

As such, ONoCs based on photonic integrated circuits (PICs) emerge as a next-generation solution to keep up with the ever-increasing demand of multi-core architectures and SoCs [7]. ONoCs offer a number of advantages. They are robust against electromagnetic noise, have a lower propagation delay, and are beneficial in terms of power consumption [7]. Furthermore, due to wavelength-division multiplexing (WDM), high-bandwidth and contention-free data transmission is possible [10], as it allows for the simultaneous transmission of multiple optical signals at different wavelengths over a single optical fiber [11].

Different architectures for ONoCs have been proposed in literature, one of which is a wavelength-routed ORNoC ([7], [12]). The ORNoC is wavelength-routed, because in contrast to traditional routing, where a segment of the message includes the destination address, the selected wavelength dictates the destination address [7].

While several efficient ONoCs architectures have been proposed in theory, their performance still needs to be simulated and evaluated in a practical environment. According to Green et al. [9] PICs have gone through a notable development. They have the capability to confine light within sub-micron dimensions, facilitation the creation of ultra-compact optical components for various functions within optical networks. These components are modulators, switches, wavelength division (de)multiplexers, filters, delay lines, detectors and fiber couplers for on/off-chip optical signal coupling, that can be combined to PICs and be test in sophisticated simulators.

In the following, an ORNoC as described in Le Beux et al. [7] will be implemented in one of these sophisticated simulators. The network should initially connect four nodes, which models four connected processor cores in a multi-core architecture or four functional components in a SoC. To achieve correct transmission behavior between transmitting and receiving nodes, the properties of the network's components, e.g. laser powers, will be adjusted accordingly. Important performance factors, such as power and signal-to-noise (SNR) ratio, are examined.

Consequently, the aim of this work is the implementation, optimization and analysis of a full functioning four-node ORNoC with full connectivity using a simulation software for PICs. First, the theoretical background of PICs, the ORNoC architecture and its design aspects are presented. Next, a simulator is chosen and its primitive elements are explained. Using these primitive elements, two possible configurations for a four-node ORNoC are presented. Finally, these configurations are simulated in multiple runs with different component properties. The corresponding results are discussed and compared.

2. Theoretical Background

2.1. Photonic Integrated Circuits

A PIC is an IC that integrates multiple photonic functions, such as generation, modulation, transmission, amplification, and detection of light; similar to electronic ICs, that manipulate electrical signals, PICs manipulate light signals for various applications [13]. One of the main applications of PICs are on-chip interconnects for high-performance multi-core processors [9], because optical links circumvent the capacitive, resistive and signal integrity constraints imposed upon electronics [6]. Multiple photonic components are required for ORNoCs. In the following, relevant components are described in accordance with [6], [10] and [14].

Waveguides are used for directing light within the boundaries of a chip. In case of off-chip lasers, couplers are required to direct light from a fiber onto the chip or from the chip into a fiber.

Optical ring resonators (ORR) make on-chip WDM possible. When connected to a waveguide, they function as notch filters. Wavelengths on resonance are trapped in the ring and can potentially be redirected onto another waveguide, while other non-resonating wavelengths pass by. The resonant wavelength of an ORR is adjusted by changing the component's geometry and/or index of refraction.

Optical ring modulators (ORM) are used to perform electro-optical conversion. An optical signal of a specific wavelength, generated by a laser, is amplitude-modulated by moving the ORM's resonance frequency in and out of the laser wavelength. This is done by electrically tuning the ORM's index of refraction.

ORRs and ORMs are described mathematically in detail, e.g. in [15]. Two formulas are relevant in the course of this work. Light is on resonance with the ring, when its wavelength fits a whole number of times inside the optical length of the ring. The resonance frequency of a ring modulator or resonators is thus given as

$$\lambda_{\text{res}} = \frac{n_{\text{eff}} \cdot L}{m}, m = 1, 2, 3... \tag{2.1}$$

where n_{eff} is the effective index of the waveguide and L the roundtrip length (circumference) of the ring.

The wavelength range between two resonances is called free spectral range (FSR).

$$FSR = \frac{\lambda^2}{n_g \cdot L} \tag{2.2}$$

where n_g is the group index of the waveguide.

Photodetectors are used for the opto-electronic conversion of optical power into an electrical current. It detects the amplitude of an optical signal at a certain frequency.

Using these components, Werner, Navaridas and Luján [10] present the arrangement of general ONoCs. A simple transmitter-receiver-pair is illustrated in Figure 2.1a. Here, an off-chip laser source generates light with the wavelengths λ_1 to λ_n. The light is coupled into an on-chip waveguide via a single mode optical fiber. The transmitter modulates the light via multiple ring modulators with different resonance wavelengths, while the receiver couples out light via multiple ring resonator/photodetector pairs with different resonance wavelengths. The steps of optical data transmission are summarized in Figure 2.1b. On the transmitting side, after encoding electronic data for error correction and signal conditioning purposes, data is serialized and provided through a driver to the optical modulator, where bits are modulated onto the modulator's optical resonance wavelength. At the receiving side, a photodetector converts light of the ORR's resonance frequency into an electrical current, which is amplified, deserialized and decoded.

Here, the laser source is located off-chip. However, there are also ONoCs with on-chip lasers. As discussed in [16], on-chip lasers avoid coupling losses, provide more flexibility during placement and allow for an improved energy efficiency. In fact, on-chip lasers are used in the underlying ORNoC architecture.

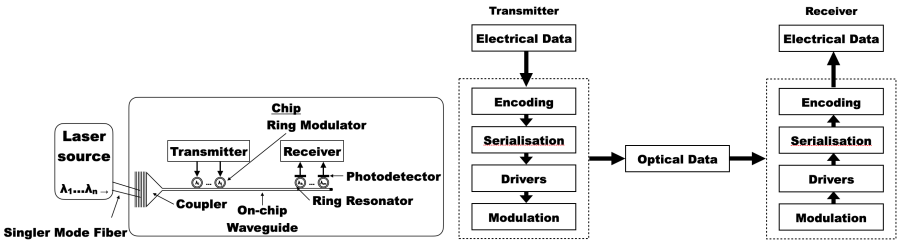

(a) Physical View **(b)** Virtual View

Figure 2.1.: Optical data transmission.

2.2. Architecture

In a wavelength-routed ORNoC all transmitters are able to communicate with all receivers simultaneously without any conflict [12]. This is based on WDM, which allows for the simultaneous transmission of multiple optical signals at different wavelengths over a single optical fiber [11]. As such, contention-free communication between all transmitting and receiving nodes is possible and arbitration is not required [12].

As described in Le Beux et al. [7], in an ORNoC electrical computing nodes (i.e. cores or functional components) are interconnected through a network that involves on-chip-lasers, waveguides, ORMs, ORRs etc. Computing nodes are represented as optical network interfaces (ONIs).

An ONI comprises an electrical and an optical portion. Data serialization and modulation together with a selection of the correct wavelength-waveguide pair is done by the electrical portion of the ONI's transmitting part. Analog-to-digital signal conversion, serialisation and storage of data in a buffer dedicated to the particular wavelength is done by the electrical portion of the ONI's receiving part.

The optical portion of an ONI, shown in Figure 2.2, comprises n_r ORRs and n_t ORMs, where each ORR is characterized by a distinct resonance wavelength λ_{ri} (receiver) and each ORM by a distinct modulated wavelength λ_{tj} (transmitter). The receiver part allows two modes of operation:

- *ejection mode*: a signal of wavelength λ_s will couple into a resonator of the ONI if $\lambda_s = \lambda_{ri}$ $(i = 0, \ldots, n_r - 1)$.
- *pass through mode*: a signal will not couple into a resonator and passes through the ONI if $\lambda_s \neq \lambda_{ri}$ $(i = 0, \ldots, n_r - 1)$.

The transmitter part adds a third mode of operation

- *inject mode*: Via a driver data is coupled into an appropriate modulator. The modulator then sends a signal into the waveguide.

Here, λ_b and λ_g are coupled into the receiver part, λ_r passes through the ONI, and λ_g and λ_p are coupled into the waveguide (grey). Further, in the example the ONI reuses the wavelength λ_g for receiving and transmitting data.

2.3. Design Aspects

Werner, Navaridas and Luján [10] and Ortín-Obón et al. [12] list important design aspects of ORNoCs. Below, a selection of those design aspects, which are important in the course of this work, are listed.

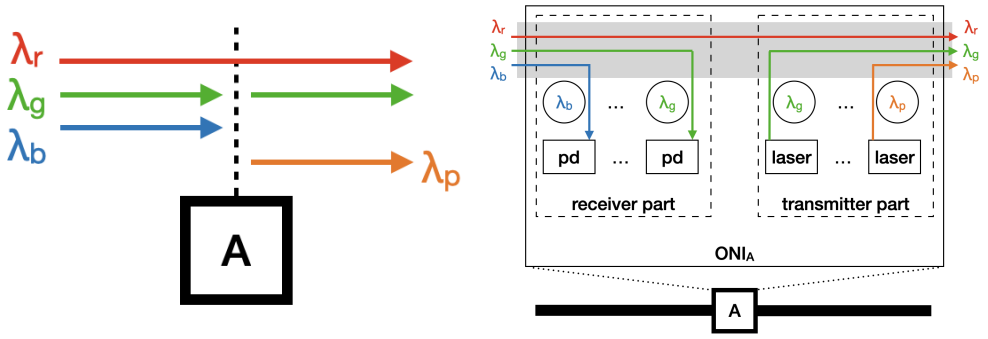

(a) Virtual View **(b)** Physical View

Figure 2.2.: A (micro-)resonators in the optical portion of an ONI.

First of all, propagation delay and latency can be considered. Optical signals in silicon waveguides propagate much faster than electrical signals in optimally repeated wires. However, optical signals require three clock cycles (electro-optical conversion, signal propagation and opto-electronic conversion), while electrical signals only require one clock cycle for data transmission, such that the latency is higher. Since this work focuses on the optical part of the ORNoC, only the propagation delay is considered.

The number of ring waveguides (*SDM degree*) and number of wavelengths per waveguide (*WDM degree*) are also of importance. A right combination of these parameters has to be found. On the one hand, because the number of wavelengths is technologically limited [7]. On the other hand, because - according to calculations performed in [10] using the NoC model DSENT [6] - the relationship between laser power and number of wavelengths is rather exponential. This is caused by increased losses in *pass through* mode of ORRs and crosstalk noise. Crosstalk is undesired mode coupling between and within silicon waveguides and resonators, which weakens optical signal powers and thus reduces signal-to-noise ratios.

In addition to losses in *pass through* mode of ORRs, other optical path losses have to be considered. Degradation of the optical signal due to losses in PIC components requires that the laser sources increase its output powers to sufficiently drive all receivers at acceptable bit-error rates.

3. Method

3.1. Simulator

The following section provides reasons for the choice of the simulator employed for this work, and a comprehensive overview of essential components drawn from its primitive element library.

3.1.1. Simulator selection

There were three programs to choose from: COMSOL Multiphysics [17], Synopsis OptSim [18], and Ansys Lumerical INTERCONNECT [19]. All three simulators can in theory be used to simulate PICs.

COMSOL Multiphysics is primarily a finite element analysis software for simulating various physical phenomena. The electromagnetic module provides capabilities to solve Maxwell's equations, which is required to examine light propagation and interaction with structures. It is best suited to simulate individual components. Simulating PICs, however, would require time-consuming preparation, modeling all important components in terms of geometry, material, meshing, setting up boundary conditions etc. As such, the simulator was ruled out.

In contrast, Synopsis OptSim and Ansys Lumerical INTERCONNECT are primarily PIC simulators that already provide models of important photonic components such as waveguides, resonators and couplers. Therefore these simulator are more suitable. Due to an unfixable technical issue that affects Synopsis OptSim, Ansys Lumerical INTERCONNECT was chosen for the simulations.

3.1.2. Primitive elements

In the following, relevant Ansys Lumerical INTERCONNECT elements are described in detail. A complete list of all properties, the corresponding default values and a port description can be found at [20].

Pseudo-Random Bit Sequence Generator (PRBS)

The pseudo-random bit sequence generator element generates a pseudo-random bit sequence and a corresponding digital signal [21]. Its most important property is its bitrate.

Data Recovery (DIG)

The data recovery element samples the input electrical signal and produces a bit sequence [22]. It can thus be used as simplified model for analog to digital conversion. To decide, for which values at the input the output is zero or one, the „threshold table“ is used.

Non-Return to Zero Pulse Generator (NRZ)

Using the digital signal from e.g. a PRBS Generator the non-return to zero pulse generator generates a sequence of non-return to zero pulses [23]. The „bias“ property sets the DC offset of the output signal and thus the signal level for encoded zeros, the „amplitude“ property sets the relative amplitude with respect to the bias to encode ones.

Continuous Wave Laser (OCL)

Lumerical INTERCONNECT provides multiple laser models. The simplest model is the continous wave laser which generates an optical signal with a constant amplitude at a specific frequency [24]. Among other things frequency and power are adjustable.

PIN Photodetector (PD)

The PIN photodetector is a photodiode featuring a broad insintric semiconductor region positioned between the p-type and n-type semiconductor regions [24]. Key properties are the central frequency, responsivity and some noise options.

Electrical Amplifier (AMP)

The electrical amplifier element is a radio frequency power amplifier which transforms a low-power radio frequency signal into a higher power signal, usually introducing additional noise in the process [25]. Most importantly gain and noise can be tuned.

Analyzer (OSC, LGCA, OSA, OCN, ONA)

- Oscilloscope element (OSC): an electrical signal in time domain [26]
- Logic Analyzer element (LGCA): a digital signal in time domain [27]
- Optical Spectrum Analyzer element (OSA): the magnitude of an optical signal vs. frequency [28]
- Optical Channel Analyzer element (OCN): the signal power and SNR of predefined channels [29]
- Optical Network Analyzer element (ONA): determines important measures including transmission vs. frequency and gain vs. frequency [30]

Optical Ring Modulator (ORM)

In Ansys Lumerical INTERCONNECT, ORMs can be represented by a composition of primitive elements, including phase shifters, waveguides and couplers [31]. Alternatively, the INTERCONNECT element library provides an ORM primitive element. For the purpose of this work, it is sufficient to use this primitive element. It modulates an optical signal at a chosen frequency depending on an electrical signal [32].

The ORM can be characterized in frequency domain and time domain. To analyze the ORM in frequency domain, a DC source of amplitude 0.6 modulates an ORM that is connected to an ONA (Figure 3.1a). The ORM's properties are extracted from the setup of [33], that uses element parameters from a known process design kit. The most important properties are listed in Table 3.1.

The transmission response recorded by the ONA (Figure 3.1b) shows that the signal with a wavelength around 1310 nm is isolated out.

To analyze the ORM in time domain, the setup shown in Figure 3.2a is used. The ORM has the same properties as described in Table 3.1. Here, the "time variant digital filter" property is of importance. The operation type of the internal time varying digital filter determines the model with which the ORM is simulated with - a static, quasi-static, or full dynamic model.

[31] explains these models in detail. In a static model the transmission function, representing the relationship between the input and through port, depends on the

Table 3.1.: Relevant properties of the ORM element.

Property	Description	Value
frequency	Modulation frequency	1310 nm
length	Waveguide length	60 µm
loss	Waveguide loss	7 dB/m
group index	Waveguide group index	4.42
coupling coefficient 1	Power coupling coefficient corresponding to the first coupler.	0.1
coupling coefficient 2	Power coupling coefficent corresponding to the second coupler.	0.1
time variant digital filter	Operation type of the internal time varying digital filter	disabled

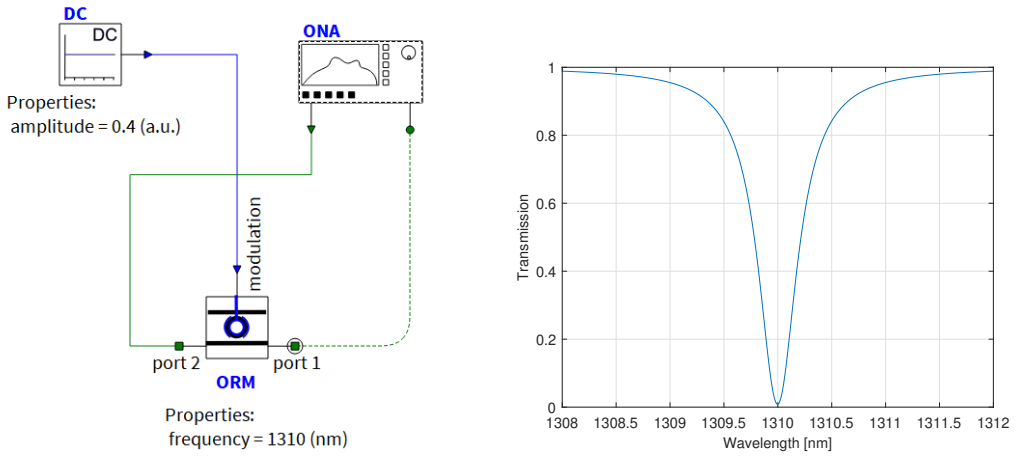

(a) Setup **(b)** Transmission Response

Figure 3.1.: Frequency domain characterization of an ORM.

modulation voltage at a particular frequency of operation. This model does only compute device behavior at the device's operating frequency. In a quasi-static model a time-varying frequency transfer function is used. As such, the ring modulator can also be utilized as a filter or multiplexer device when cascading multiple ring modulators. However, the quasi-static model does not consider cavity dynamics of an ORM. Cavity dynamics cause and overshoot and ring-down behavior (see "disabled" curve in Figure 3.3). When the cavity is on resonance, optical energy accumulates in the high Q ring, which is released when the cavity is detuned. Depending on the input modulation speed and quality factor of the modulator, these dynamics may be ignored.

The full dynamic model is only applied if the "time variant digital filter" property is set to "disabled", which was done in Figure 3.2b. In this work, it is sufficient to use the simplified model that excludes cavity dynamics. For this, the "time variant digital filter" property "update" or "interpolate" can be utilized.

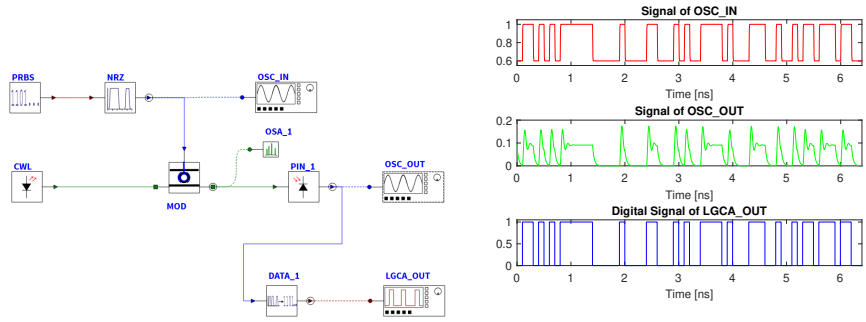

(a) Setup **(b)** Results

Figure 3.2.: Time domain characterization of an ORM.

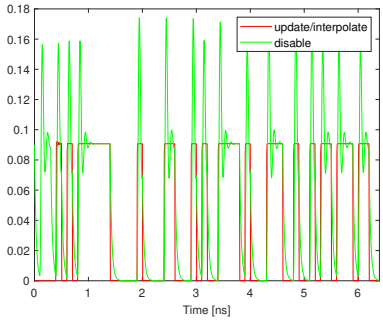

Figure 3.3.: Signal of OSC_OUT for the property "time variant digital filter" set to "interpolate/update" or "disable".

Double Bus Ring Resonator (ORR)

Like ORMs, ORRs can be represented by primitive elements, i.e. waveguides and couplers [34]. However, for simplification purposes the double bus ring resonator from the INTERCONNECT element library is utilized in this work. The element couples light at resonance; it consists a drop port for the part of the optical signal that is coupled out of the waveguide and a pass port for the part of the optical signal that passes through [35].

It is sufficient to characterize the ORR in frequency domain. For this, the ORR's drop port (bottom left port) and the pass port (top right port) are connect to an ONA (Figure 3.4a). As for the ORM, the ORR's properties are extracted from the setup of [33]. The most important properties are listed in Table 3.2.

Table 3.2.: Relevant properties of the ORM element.

Property	Description	Value
frequency	Modulation frequency	1310 nm
length	Waveguide length	60 µm
loss 1 & 2	Waveguide loss	7 dB/m
group index	Waveguide group index	4.42
coupling coefficient 1 1 & 2	Power coupling coefficient corresponding to the first coupler.	0.1
coupling coefficient 2 1 & 2	Power coupling coefficent corresponding to the second coupler.	0.1

The gain spectrum of the drop port and through port recorded by the ONA Figure 3.1b shows that the signal with a wavelength around 1310 nm is filtered out.

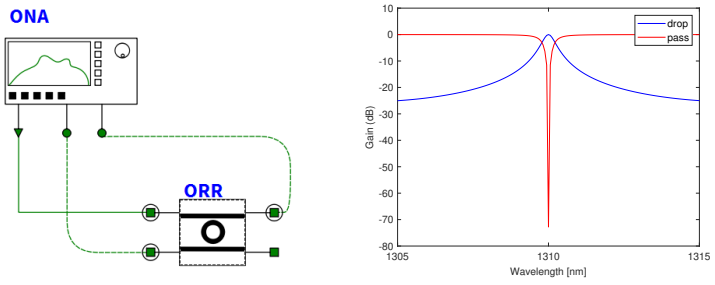

(a) Setup **(b)** Gain spectrum

Figure 3.4.: Frequency domain characterization of an ORR.

3.2. ORNoC Configurations

The ORNoC was designed in accordance with Le Beux et al. [7]. The network consists of four nodes (ONIs) which are interconnected with at least one waveguide. Simulations were performed with Ansys Lumerical INTERCONNECT 2024 R1. A general description of the components of the simulation setup is done. Each configuration is simulated for multiple setups with different element properties. For each setup, all non-default values are given in Appendix A.

3.2.1. Optimization of ORMs and ORRs

The following setups, based on an example about WDM on the Ansys website [33], were used to optimize the properties of the ORMs and ORRs employed in the configurations of subsection 3.2.2 and subsection 3.2.3.

To optimize the ORM's parameters the circuit of Figure 3.5a was used. The output of *ONA_2* is divided equally via the ideal splitter *SPLIT* and fed into the input of seven parallel ORMs (*ORM_f1* to *ORM_f7*). The modulation port of the ORMs is left unconnected and their output monitored by *ONA_2*. Each ORM is characterized by a different resonance frequency.

The circuit of Figure 3.5b was used to examine the amplitude-depended off-resonance shift of the ORM's transmission curve due to modulation. With this circuit the channel spacing can be determined.

To optimize the ORR's parameters the circuit of Figure 3.5c was used. Here, the ORRs are arranged in series: the output of *ONA_1* is fed into the input of *ORR_f1*. Its output is connected to the input of *ORR_f2* etc. The output port of *ORR_f7* is examined by *ONA_1*.

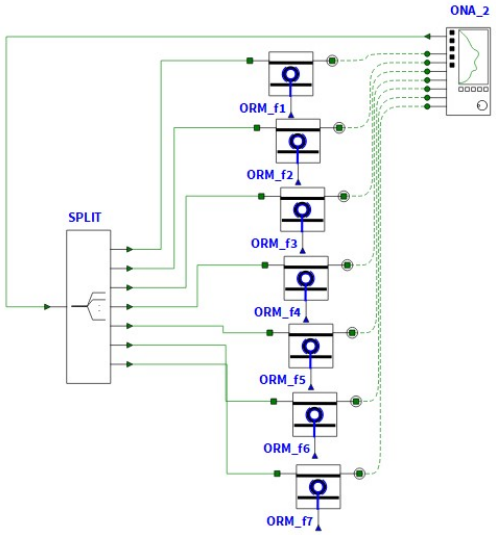

(a) ORM Setup

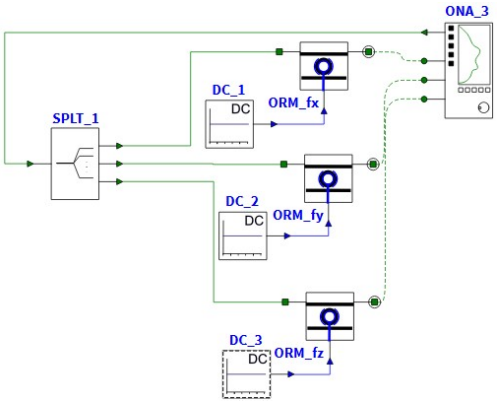

(b) ORR Setup

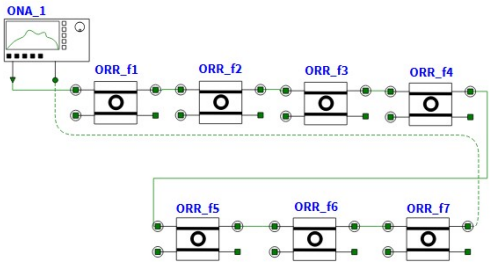

(c) ORR Setup

Figure 3.5.: Setups to optimize the ORM's and ORR's parameters.

3.2.2. First Configuration

Figure 3.6 shows the first configuration in a virtual view (Figure 3.6a) and a physical view (Figure 3.6b). As can be seen, one waveguide is used to connect the four nodes. One waveguide is sufficient to connect four nodes, because seven frequencies/wavelengths are required for full connectivity, which is below the technological limit described in [7].

In the virtual view, the color of each arrow indicates the frequency/wavelength used to connect the two nodes. For example, node A and node C are interconnected by a yellow arrow, which indicates that frequency f_2 is used to connect these two nodes. Table 3.3 lists via which frequency two nodes are connected.

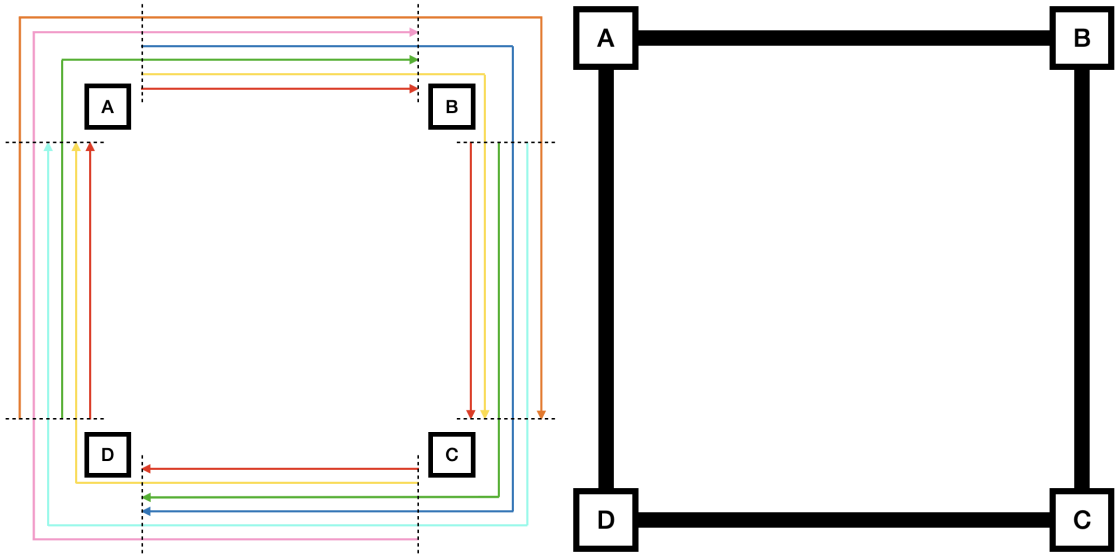

(a) Virtual View **(b)** Physical View

Figure 3.6.: First Configuration, Topology

Table 3.3.: Connectivity Matrix for the first configuration (transmitter in row, receiver in column).

	A	B	C	D
A		f_1	f_2	f_4
B	f_5		f_1	f_3
C	f_2	f_6		f_1
D	f_1	f_3	f_7	

A corresponding top-level Lumerical INTERCONNECT simulation setup is shown in Figure 3.7. Waveguide elements are not used. Due to their short length on microchips their effect on the simulation results are negligible. For the sake of clarity, four optical attenuators [36] with 0-db attenuation are located between the different nodes.

Figure 3.7b shows the node ONI_A. Each node consists of three receivers (here Rx_{f1}, Rx_{f2} and Rx_{f5}), three transmitters (here Tx_{f1}, Tx_{f2} and Tx_{f4}), an ideal coupler to combine the output of the receiver part with the input from the transmitter part, and an OSA and OCN at the output to observe the power of the different signals in the optical channels. With all its components the ONI models the physical view of an ONI shown in Figure 2.2b. Figure 3.7c and Figure 3.7d depict a receiver of ONI_A for frequency f_2 and a transmitter of ONI_B for frequency f_1. The models include all optical and electrical components which are needed to simulate an ORNoC as described above. Other components are excluded, such as data encoding and decoding.

The receiver of Figure 3.7c comprises an ORR *A_RES_f2*, a PIN photodetector *A_PD_f2*, an electrical amplifier *A_AMP_f2*, and a data recovery element *A_DIG_f2*. Furthermore, to analyze and measure the incoming signal, two oscilloscopes *A_OSC_PD_2* and *A_OSC_AMP_2*, and a logic analyzer *A_LGCA_f2* are used.

The transmitter of Figure 3.7d comprises an ORM *A_MOD_f1*, a laser *A_OCL_f1*, a PRBS generator *A_PRBS_f1*, and a NRZ pulse generator *A_NRZ_f1*. To analyze and measure the outgoing signal, an oscilloscope *A_OSC_IN_f1*, and a logic analyzer *A_LGCA_IN_f2* are utilized.

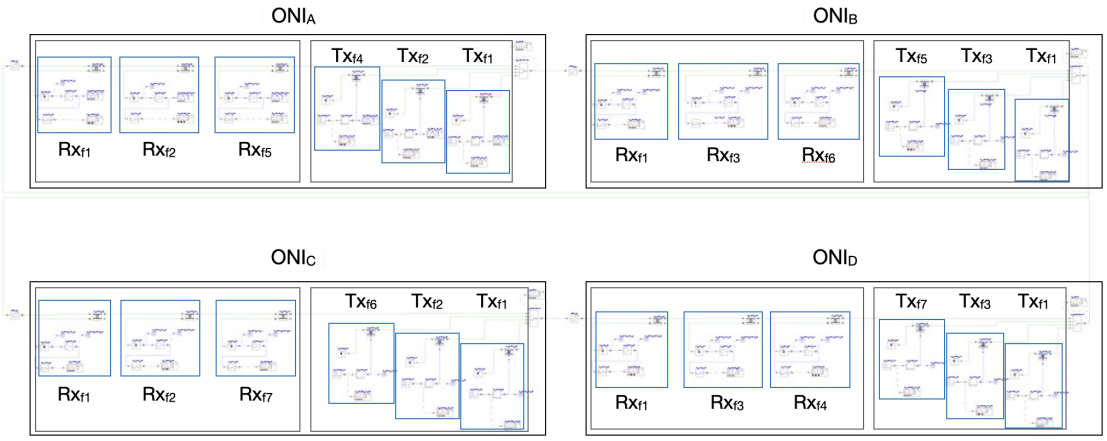

(a) Top-level view

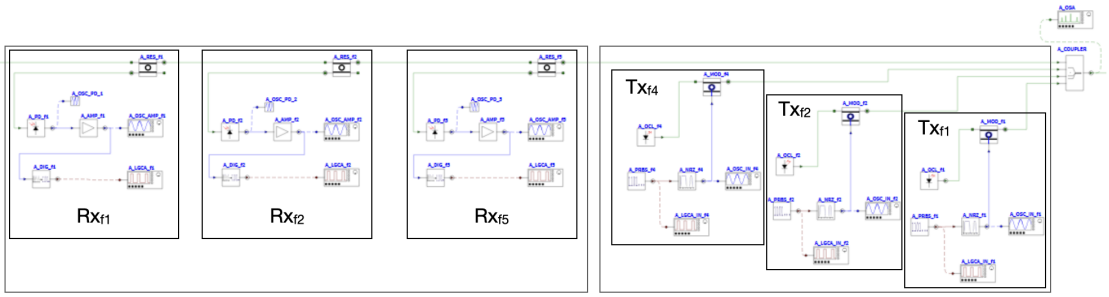

(b) ONI_A

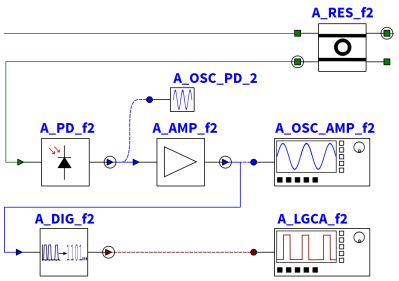

(c) Receiver of ONI_A for frequency f_2

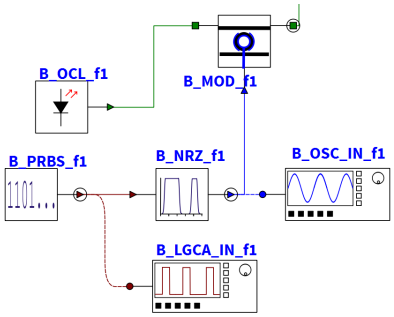

(d) Transmitter of ONI_B for frequency f_1

Figure 3.7.: First Configuration, Lumerical INTERCONNECT Schematics

3.2.3. Second Configuration

Figure 3.8 displays the second configuration in a virtual view (Figure 3.8a) and a physical view (Figure 3.8b). As can be seen, two waveguides are used to connect the four nodes. In the inner waveguide, light travels in a clockwise direction of rotation; in the outer waveguide, light has a counterclockwise direction of rotation. As such, for full connectivity, only two frequencies/wavelengths per waveguide are required. Moreover, the two frequencies/wavelengths can be chosen the same in the two waveguides.

As described above, in the virtual view, the color of each arrow indicates the frequency/wavelength used to connect the two nodes. Table 3.4 lists via which frequency two nodes are connected.

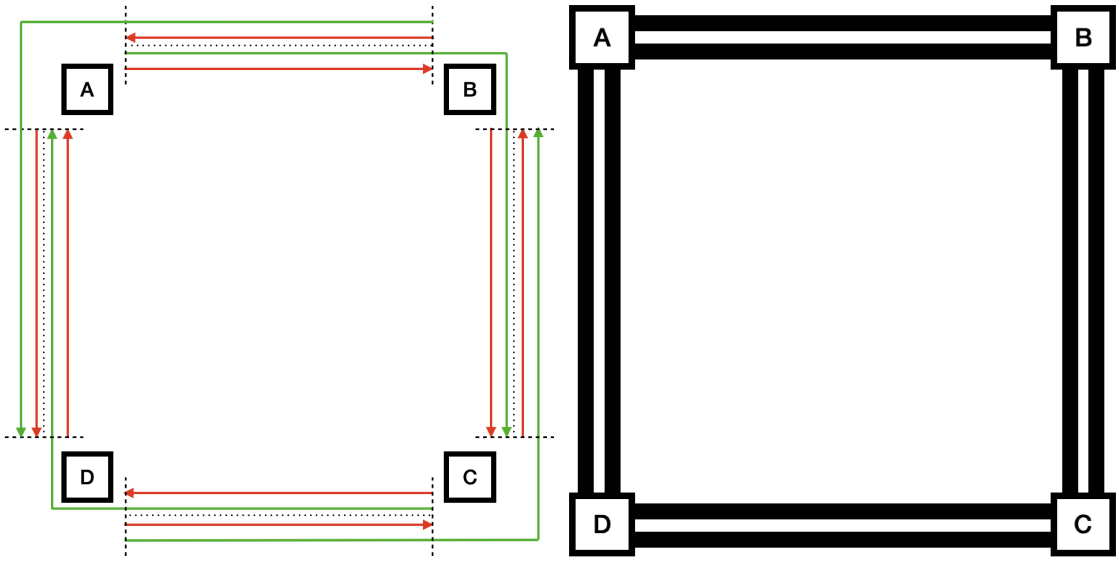

(a) Virtual View **(b)** Physical View

Figure 3.8.: Second Configuration, Topology

Table 3.4.: Connectivity Matrices for (a) the inner waveguide and (b) the outer waveguide of the second configuration (transmitter in row, receiver in column).

(a)

	A	B	C	D
A		f_1	f_2	
B			f_1	
C	f_2			f_1
D	f_1			

(b)

	A	B	C	D
A				f_1
B	f_1			f_2
C		f_1		
D		f_2	f_1	

A corresponding top-level Lumerical INTERCONNECT simulation setup is shown in Figure 3.9. Also here, no waveguide elements are used. Due to their short length on microchips their effect on the simulation results are negligible. For the sake of clarity, four optical attenuators [36] with 0-db attenuation are located between the different nodes.

Figure 3.9b shows the node ONI_A. Each node consists of three receivers (here Rx_{f11}, Rx_{f12} and Rx_{f21}), three transmitters (here Tx_{f11}, Tx_{f12} and Tx_{f21}) an ideal coupler to combine the output of the receiver part with the input from the transmitter part, and an OSA and an OCN at the output to observe the power of the different signals in the optical channels. With all its components the ONI models the physical view of an ONI shown in Figure 2.2b.

The receivers and transmitters of the second configuration comprise the same components as the receivers and transmitters of the first configuration.

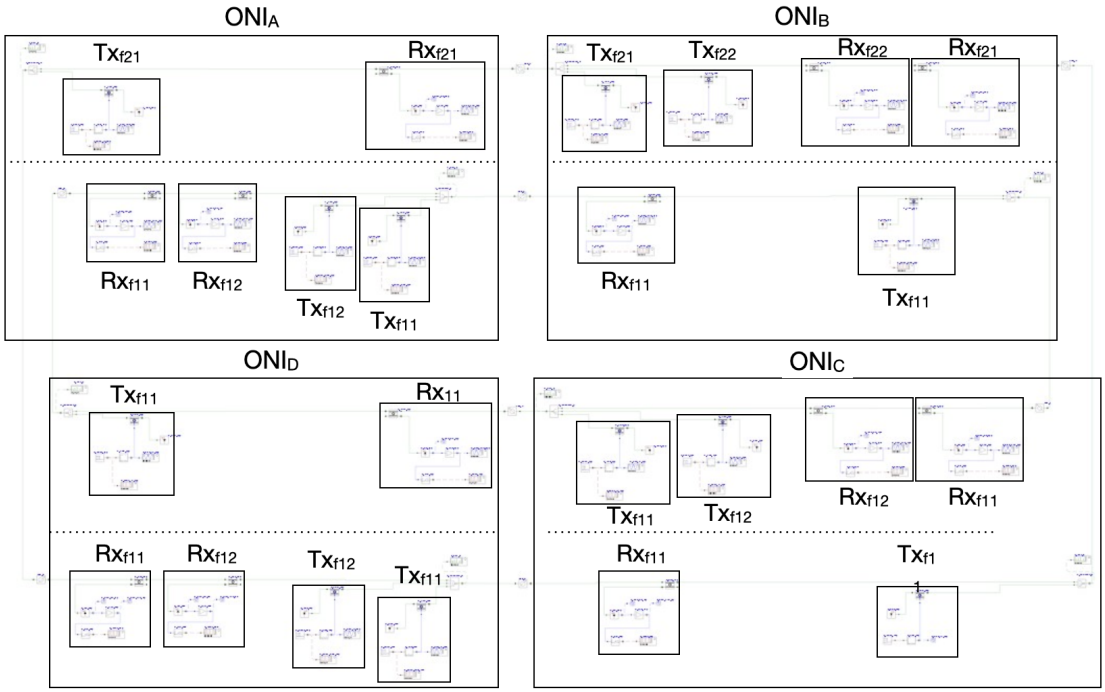

(a) Top-level view

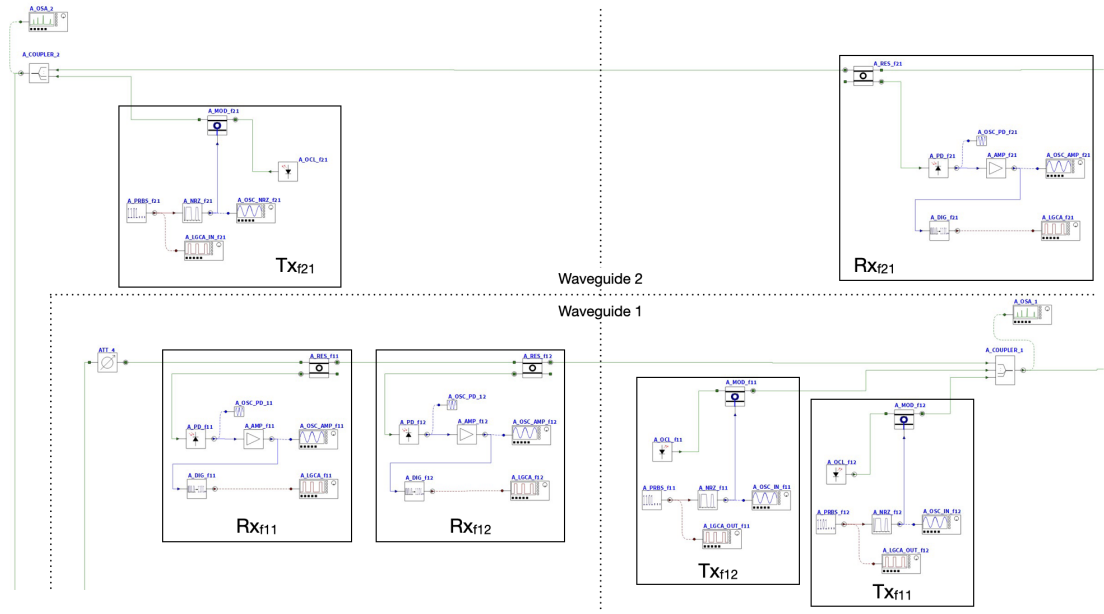

(b) ONI_A

Figure 3.9.: Second Configuration, Lumerical INTERCONNECT Schematics

4. Simulation Results

4.0.1. First Configuration

Starting with the properties given in [33], the element's parameters are adjusted. First of all, the receiving side's AMPs and PDs are set noise-free.

Setup 1

For the properties given in [33] the four OSAs (at the output of each node) show a signal pattern as shown in Figure 4.1a. Figure 3.6a and Table 3.3 can be used as an explanation for the peaks observed in the plots. Regarding ONI_A, because signals at frequencies f_3, f_6 and f_7 pass through the ONI, signals at frequencies f_1, f_2 and f_4 are ejected into the three ORRs, and signals at frequencies f_1, f_2 and f_5 are injected via the three ORMs of the transmitting side, peaks at frequencies f_1, f_2, f_3, f_4, f_6 and f_7 are observable at *A_OSA*. Analogously, the peaks for ONI_B (*B_OSA*), ONI_C (*C_OSA*) and ONI_D (*D_OSA*) can be explained.

However, a comparison between the transmitted and received signals shows that the configuration does not work as expected.

Shorter channels, i.e. those that connect neighbouring nodes, show correct transmission behaviour. For instance, the transmission from ONI_A to ONI_B via f_1 is shown in Figure 4.1b. *A_PRBS_f1* of transmitter Tx_{f1} generates the digital signal shown in the first plot. The received signal at *B_PD_f1* (second plot) shows close resemblance to the transmitted signal, but with a small amplitude ($10^{-4)}$).

Signals arriving at the receiving node of longer channels, i.e. channels that run through multiple nodes, have an even smaller amplitude and additionally are fuzzy. The transmission from ONI_A to ONI_D via f_4 as depicted in Figure 4.1c serves as an example. The signal arriving at ONI_D has an amplitude with a magnitude of 10^{-5}; the received signal at *D_PD_f4* is only partially similar to the transmitted signal.

In both cases a noisy PD and AMP would deface the signal; the noise will most likely exceed the signal. As first approach the laser power of the transmitters was increased, which could not solve the issue of fuzzy signals. This leads to the assumption that crosstalk may be the possible cause. Therefore, a suitable set of parameters for the ORRs and ORMs needs to be found.

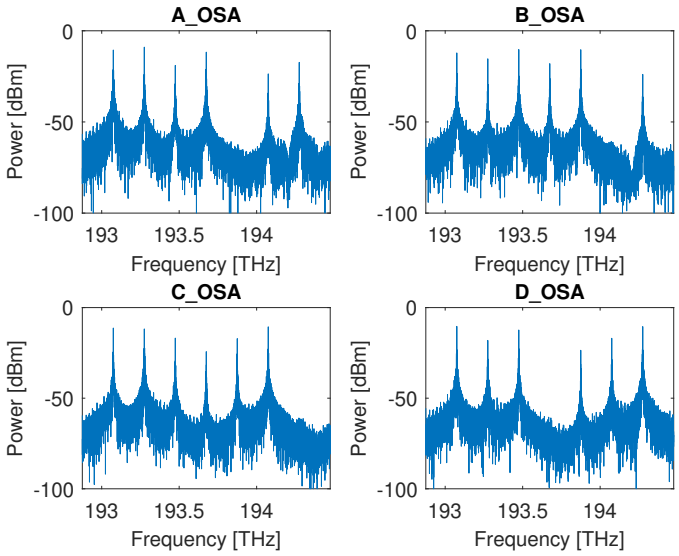

(a) Signal of all OSAs in setup 1.

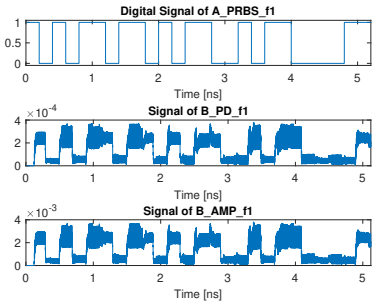

(b) ONI_A to ONI_B via f_1.

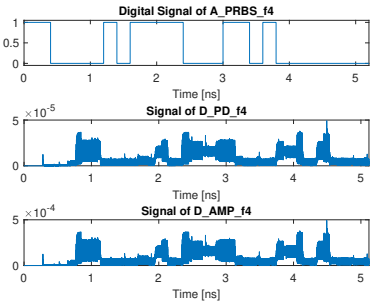

(c) ONI_A to ONI_D via f_4.

Figure 4.1.: Signals (first configuration, setup 1).

The circuits of Figure 3.5 were used to examine whether the parameters of [33] indeed allow crosstalk.

First, Figure 4.2a shows that the curve of frequency f_1 changes from 193.075 THz for 0.6 a.u. modulation amplitude to 193.195 THz for 1 a.u. modulation amplitude. Thereby the curve slightly overlaps the curve of the adjacent frequency f_2 for 0.6 a.u. modulation. Thus, even tough a change of the modulator's amplitude from 0.6 a.u. to 1 a.u. changes the refractive index sufficiently to shift the curve completely off-resonance, the shift may affect adjacent channels. Furthermore, *ONA_2* measures a FSR of approximately 1.13 THz, which is below the frequency delta (between f_{max} and f_{min})

$$\Delta f = 6 * 0.2\,\text{THz} = 1.2\,\text{THz} \tag{4.1}$$

As such, two successive minima in the ORRs and ORMs transmission/gain curves are too close together. Figure 4.2b depicts the situation. For instance, the second minimum for ORRs with resonance frequency f_1 (at 194.203 THz) is below the first minimum of ORRs with resonance frequency f_7 (at 194.275 THz) - data transmission via the channel at frequency f_1 will affect the channel at frequency f_7 and vice versa.

In summary, the ORM's and ORR's parameter choice allows crosstalk and prevents proper operation. Thus, these parameters need to be adjusted.

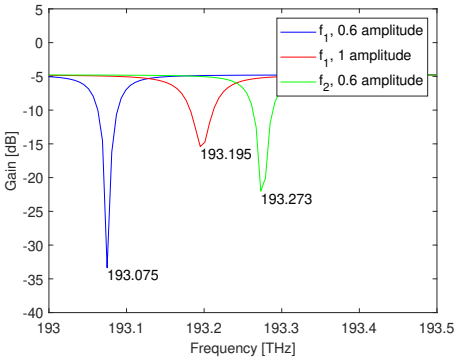

(a) Gain signals of ONA_3.

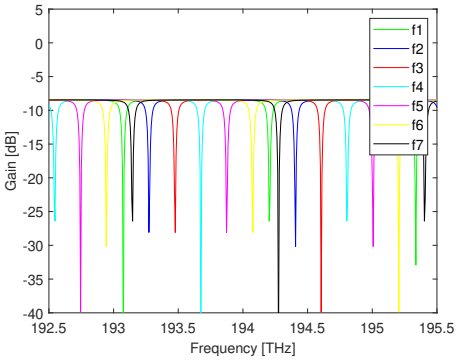

(b) Gain signals of ONA_2.

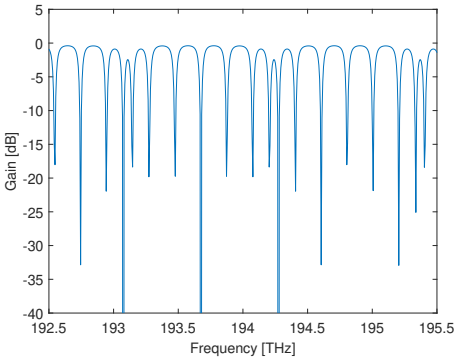

(c) Gain signals of ONA_1.

Figure 4.2.: Signals of the setups to optimize the ORM's and ORRs (first configuration, setup 1).

Setup 2

In the next setup, properties for the ORRs and ORMs were taken from [37]. The circuits of Figure 3.5 were used to verify the feasibility of these properties.

Like in the example of [33], the ORMs are modulated by a bias of 0.6 a.u. to encode zeros and and an absolute amplitude of 1 a.u. to encode ones. The curve of frequency f_1 changes from 193.099 THz for 0.6 a.u. amplitude to 193.237 THz for 1 a.u. amplitude (Figure 4.3). From this, two conclusions can be drawn. Firstly, the modulation

$$\Delta f_{mod} = 193.237\,\text{THz} - 193.099\,\text{THz} = 0.138\,\text{THz} \tag{4.2}$$

is sufficient to shift the curve completely off-resonance and as such allow data encoding with the ORR. Secondly, a frequency spacing of

$$\Delta f_{channel} = 0.3\,\text{THz} > 2 * \Delta f_{mod} = 0.276\,\text{THz} \tag{4.3}$$

can be chosen which avoids overlap with adjacent frequencies.

With the chosen frequency spacing $\Delta f_{channel}$ the use of seven channels (wavelengths) without overlap is possible because an increased FSR of 2.54 THz measured by *ONA_2* of Figure 3.5a is bigger than the frequency delta (between f_{max} and f_{min})

$$\Delta f = 6 * 0.3\,\text{THz} = 1.8\,\text{THz} \tag{4.4}$$

Displaying the measured gain of all ORMs in one plot demonstrates that there is no overlap between the gain curves of adjacent frequencies (Figure 4.3b). Plotting the output of *ORR_f7* measured by *ONA_1* shows the same (Figure 4.3c).

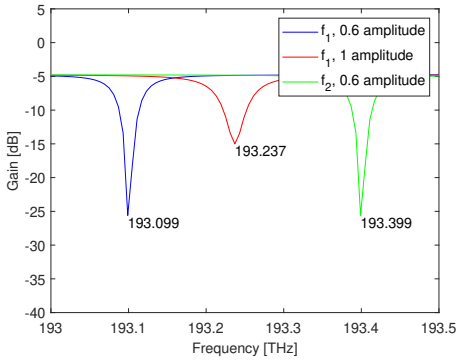

(a) Gain signals of ONA_3.

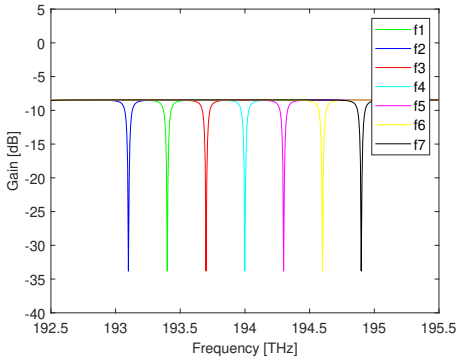

(b) Gain signals of ONA_2.

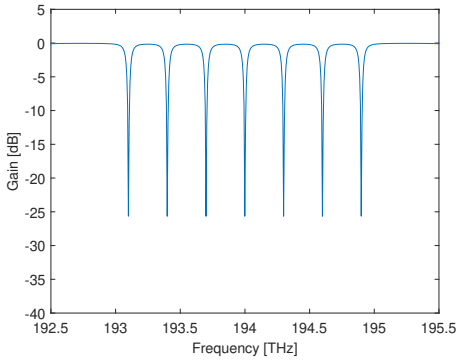

(c) Gain signals of ONA_1.

Figure 4.3.: Signals of the setups to optimize the ORMs and ORRs (first configuration, setup 2 and setup 3).

Figure 4.4a plots the measured spectra of the four OSAs (at the output of each node) for setup 2. An explanation for the peaks is given in setup 1.

Here, short and long channels show correct transmission behavior. For instance, the transmission from ONI_A to ONI_B via frequency f_1 is shown in Figure 4.4b. *A_PRBS_f1* of transmitter Tx_{f1} generates the digital signal shown in the first plot. The received signal at *B_PD_f1* (second plot) shows close resemblance to the transmitted signal, but still with small amplitude ($10^{-4)}$). In comparison to setup 1 the signal is less fuzzy.

In the transmission from ONI_A to ONI_D via frequency f_4 (Figure 4.4c), the transmitted signal is fully recognisable with low amplitude ($10^{-5)}$) at the receiving node. Zeros are clearly distinguishable from ones. The delay for sending data through multiple nodes is apparent.

In addition to the adjustment of the ORRs' and ORMs' properties, the threshold table of the data recovery elements was modified in order to obtain the received signals correctly in digital domain. Data recovery elements of the Rx_{f1} receivers can fully reconstruct the transmitted digital signal with a threshold of 0.001 a.u. for ones. A threshold of 0.0003 a.u is used for the data recovery elements of the Rx_{f2} and Rx_{f3} receivers. All further data recovery elements (of receivers Rx_{f4}, Rx_{f5}, Rx_{f6} and Rx_{f7}) were assigned a threshold of 0.0001 a.u. to allow proper signal reconstruction.

Signal power and SNR for all relevant frequencies at the input of each node are listed in Table 4.1. The values were obtained using an OCN element and verified using the OSA's measured spectra. In this context, a relevant frequency is a frequency that is part of the ONI's receiving side. For instance, Table 4.1b lists the channels f_1, f_3 and f_6 that are received by the ORRs of ONI_B. As expected, with channel length-independent laser power, frequencies of shorter channels have a higher signal power than frequencies of longer channels at the receiver. In contrast, the SNR is not (indirectly) proportional to the channel length. This may be due to the fact that the signals preserve their shape but loose overall power as they pass through the ORRs (modelled by the "loss" parameters).

To achieve a sufficient signal power at the input of an ONI, such that signals can be reconstructed correctly even in the presence of noise at the PDs and AMPs, laser powers need to be adjusted. As such, in the next setup, the noise of the elements is activated and the laser power of longer channels is increased.

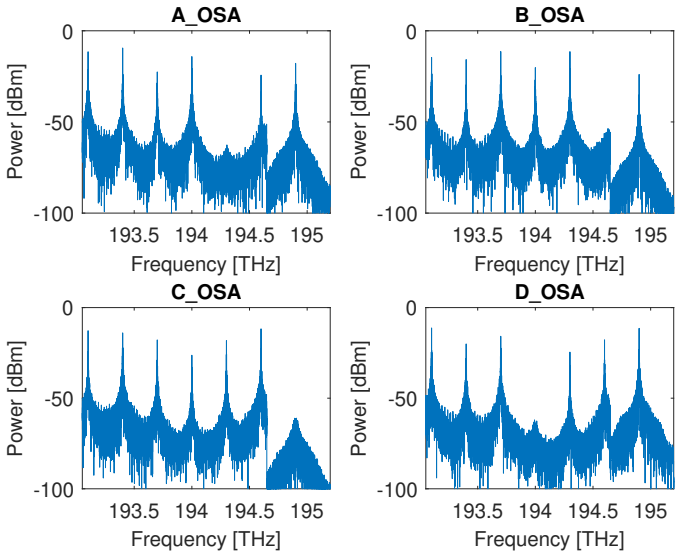

(a) Signal of all OSAs in setup 2.

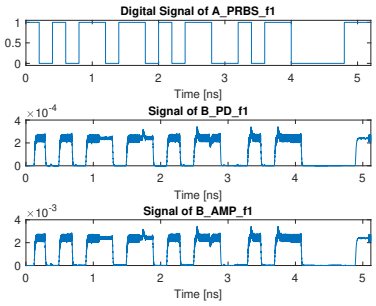

(b) ONI_A to ONI_B via f_1.

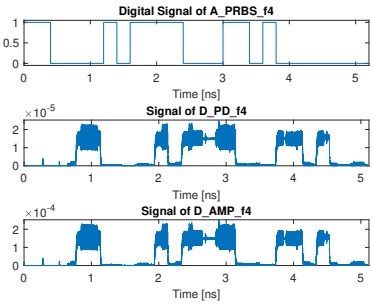

(c) ONI_A to ONI_D via f_4.

Figure 4.4.: Signals (first configuration, setup 2).

	Signal Power	SNR
f_1	−9.09 dBm	17.78 dB
f_2	−16.83 dBm	14.76 dB
f_5	−21.73 dBm	19.10 dB

(a) ONI_A

	Signal Power	SNR
f_1	−9.31 dBm	16.26 dB
f_3	−18.00 dBm	16.33 dB
f_6	−21.74 dBm	16.92 dB

(b) ONI_B

	Signal Power	SNR
f_1	−10.96 dBm	17.21 dB
f_2	−14.24 dBm	19.42 dB
f_7	−21.54 dBm	16.60 dB

(c) ONI_C

	Signal Power	SNR
f_1	−9.98 dBm	16.97 dB
f_3	−15.37 dBm	17.70 dB
f_4	−22.66 dBm	17.80 dB

(d) ONI_D

Table 4.1.: Signal powers and SNRs (first configuration, setup 2).

Setup 3

In this setup, thermal noise and shot noise are present in PDs, and a noise figure of 3 dB characterizes the AMPs. The presence of noise requires increasing the laser powers. Further, the aim is to obtain approximately similar signal powers at the nodes' inputs, such that the amplitude of the received signals is similar and the DIG elements can therefore be assigned the same threshold.

The power of lasers injecting light into short channels (frequency f_1) is set to 3 mW, the power of lasers injecting light into mid-range channels (frequency f_2 and f_3) to 15 mW and the power of lasers injecting light into long-range channels (frequency f_4, f_5, f_6 and f_7) to 50 mW, such that total laser power is

$$P_{tot} = 4 * 3\,\text{mW} + 2 * 15\,\text{mW} + 2 * 15\,\text{mW} + 4 * 50\,\text{mW} = 272\,\text{mW} \tag{4.5}$$

Figure 4.5a plots the measured spectra of the four OSAs (at the output of each node) for setup 3. In contrast to the spectra of setup 2, the peaks at transmitting frequencies are higher, which is a result of higher laser powers.

Upon considering the transmission behaviour from ONI_A to the other nodes, the noise added by PD and AMP becomes visible. Choosing laser powers too low would make it impossible to distinguish between zeros and ones. In this setup, as can be seen by comparing the transmitted signal of the PRBS elments and received signal at the output of the AMPs, the transmission from ONI_A to ONI_B (Figure 4.5b), ONI_C (Figure 4.5c) and ONI_D (Figure 4.5d) is correct.

Moreover, the received signals all have an amplitude of approximately 0.01 a.u. after amplification, because signal powers at the input of the nodes are similar (Table 4.2).

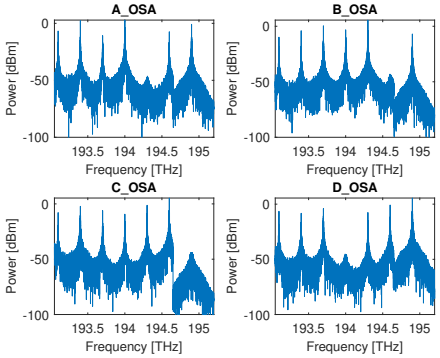

(a) Signal of all OSAs in setup 1.

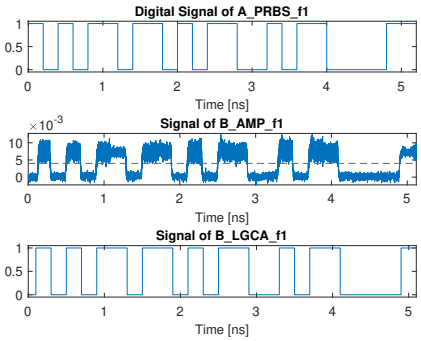

(b) ONI_A to ONI_B via f_1.

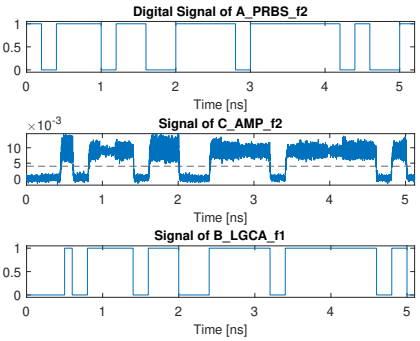

(c) ONI_A to ONI_C via f_2.

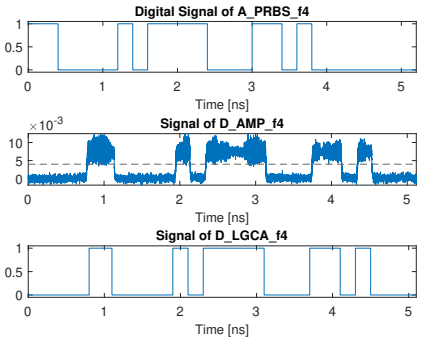

(d) ONI_A to ONI_D via f_4.

Figure 4.5.: Signals (first configuration, setup 3).

	Signal Power	SNR
f_1	−4.31 dBm	17.80 dB
f_2	−5.07 dBm	14.76 dB
f_5	−4.74 dBm	19.13 dB

(a) ONI_A

	Signal Power	SNR
f_1	−4.55 dBm	16.23 dB
f_3	−6.23 dBm	16.33 dB
f_6	−4.77 dBm	17.92 dB

(b) ONI_B

	Signal Power	SNR
f_1	−6.19 dBm	17.16 dB
f_2	−2.48 dBm	19.42 dB
f_7	−4.55 dBm	16.60 dB

(c) ONI_C

	Signal Power	SNR
f_1	−5.15 dBm	16.48 dB
f_3	−3.61 dBm	17.70 dB
f_4	−5.67 dBm	17.84 dB

(d) ONI_D

Table 4.2.: Signal powers and SNRs (first configuration, setup 3).

As such, the threshold value of all DIG elements can be set to 0.004 a.u. (depicted in the AMP's plots of Figure 4.5 as dashed lines) and the signal be reconstructed correctly in digital domain.

It is further evident, that longer channels are characterized by a higher transmission delay. The delay for short channels (e.g. ONI_A to ONI_B) is 0.1 ns, for mid-range channels (e.g. ONI_A to ONI_C) 0.4 ns, and for long-range channels (e.g. ONI_A to ONI_D) 0.7 ns.

4.0.2. Second Configuration

Setup 1

The properties given in [33] are utilized for setup 1. Additionally, thermal noise and shot noise are present in the PDs, and a noise figure of 3 dB characterizes the AMPs. With a FSR of approximately 1.13 THz (see above) frequency f_1 can be set to 193.075 THz and frequency f_2 to 193.675 THz without crosstalk. Hereinafter, f_{11} and f_{12} refer to the frequencies/channels f_1 and f_2 of the inner waveguide (clockwise rotation direction), and f_{21} and f_{22} to the frequencies/channels f_1 and f_2 of the outer waveguide (counterclockwise rotation direction).

The circuits of Figure 3.5 provide the results shown in Figure 4.6. No overlap of the two frequencies is apparent, which verifies the correct choice of frequencies.

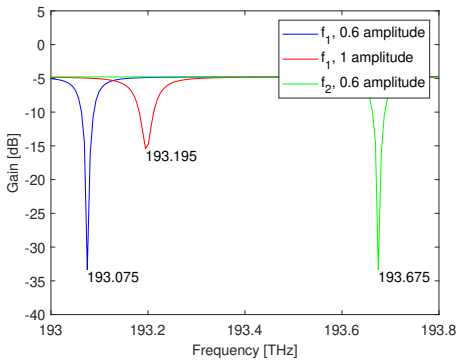

(a) Gain signals of ONA_3.

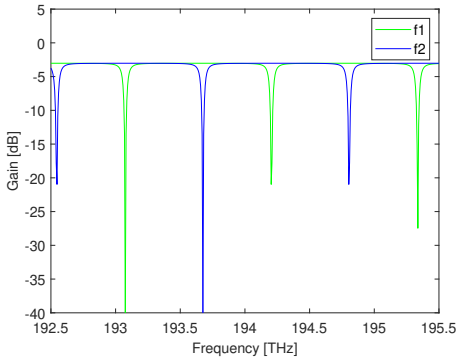

(b) Gain signals of ONA_2.

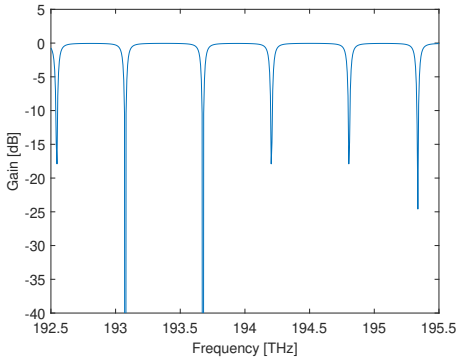

(c) Gain signals of ONA_1.

Figure 4.6.: Signals of the setups to optimize the ORM's and ORRs (second configuration, setup 1).

The measured signals of the OSAs of the inner waveguide and of the OSAs of the outer waveguide are plotted in Figure 4.7a and Figure 4.7b. At every node and waveguide, frequency f_1 and f_2 are either both injected, or only f_1 is injected and f_2 passes through the node (refer to Figure 3.8a for a visualization). In general, the values at the peaks differ only slightly, which can be explained by the lower number of channels (i.e. two per waveguide) and the shorter maximum distance between two connected nodes (i.e. signals with frequency f_2 only pass through one node). As such laser powers of frequency f_1 and f_2 only need to differ slightly to obtain equal signal powers at the ONI's inputs.

A look at the transmission behaviour (Figure 4.8) illustrates another advantage of the second configuration. Even with the parameters from [33] and in the presence of noise a reliable transmission is possible; as explained above, there is no overlap of the two frequencies' spectra. However, as illustrated in the AMPs' plots (particularly *C_AMP_f12*), it is necessary to adjust the laser powers in order to safely reconstruct the signal in digital domain.

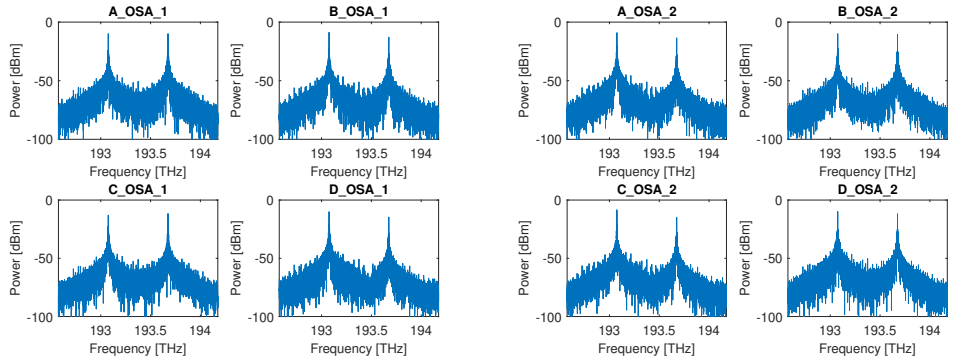

(a) Signals of the inner waveguide's OSAs. **(b)** Signals of the outer waveguide's OSAs.

Figure 4.7.: Signals recored by OSAs (second configuration, setup 1).

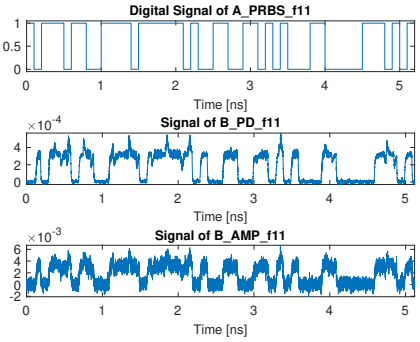

(a) ONI_A to ONI_B via f_1.

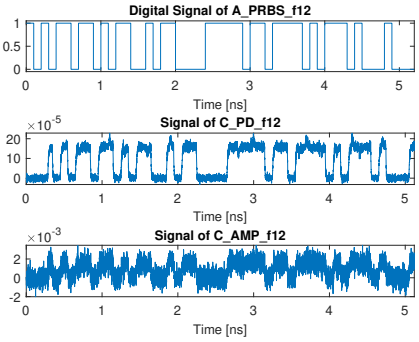

(b) ONI_A to ONI_C via f_2.

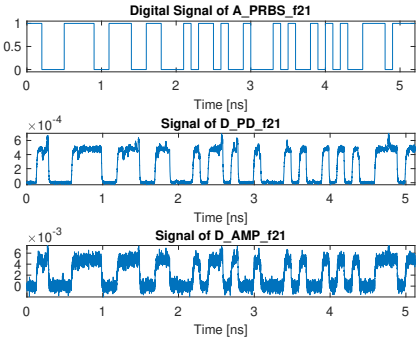

(c) ONI_A to ONI_D via f_1.

Figure 4.8.: Transmitted Signals (second configuration, setup 1).

Indeed, signal powers of the second configuration in setup 1 are generally bigger and less divergent from each other compared to the first configuration (Table 4.3). The measured SNRs are, however, lower. Despite recalculations and rigorous investigation of all parameters, the values remain the same. The observed phenomenon eludes a comprehensive explanation.

Based on the first setup, two alternative approaches are possible. The first possibility would be an adjustment of the laser powers with the properties from [33], the second possibility to employ the properties used in setup 2 and 3 of the first configuration and adjust the laser powers accordingly. Both are done in the following.

	Signal Power	SNR
f_{11}	−7.03 dBm	13.43 dB
f_{12}	−11.95 dBm	14.30 dB
f_{21}	−7.90 dBm	15.54 dB

(a) ONI_A

	Signal Power	SNR
f_{11}	−7.87 dBm	15.41 dB
f_{21}	−6.19 dBm	16.55 dB
f_{22}	−12.12 dBm	14.14 dB

(b) ONI_B

	Signal Power	SNR
f_{11}	−6.47 dBm	15.09 dB
f_{12}	−11.00 dBm	15.05 dB
f_{21}	−7.85 dBm	15.23 dB

(c) ONI_C

	Signal Power	SNR
f_{11}	−9.59 dBm	14.77 dB
f_{21}	−6.72 dBm	14.48 dB
f_{22}	−11.27 dBm	15.47 dB

(d) ONI_D

Table 4.3.: Signal powers and SNRs (second configuration, setup 1).

Setup 2

This setup uses the parameters from setup 1, but with adjusted laser powers of 2 mW for frequency f_1 and 5 mW for frequency f_2. As such, the total laser power sums up to

$$P_{tot} = 8 * 2\,\text{mW} + 4 * 5\,\text{mW} = 36\,\text{mW} \tag{4.6}$$

The frequencies itself remain unchanged at 193.075 THz and 193.675 THz respectively, which is apparent in the measured spectra of the OSAs (Figure 4.9).

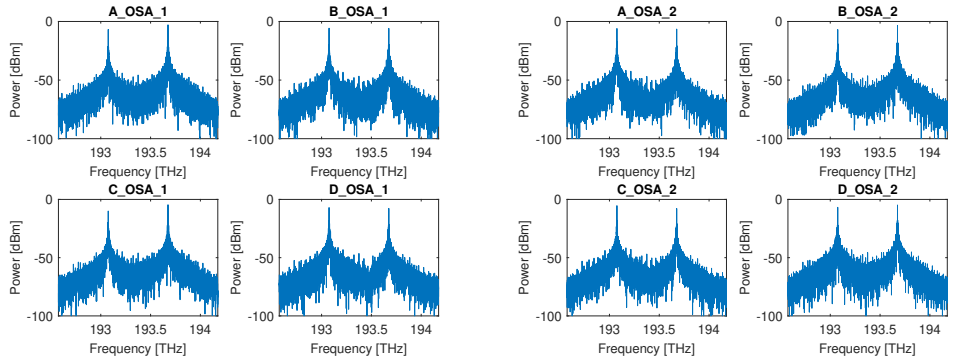

(a) Signals of the inner waveguide's OSAs. **(b)** Signals of the outer waveguide's OSAs.

Figure 4.9.: Signals recored by OSAs (second configuration, setup 2).

The transmission behavior is shown in Figure 4.10. With the increased laser powers the signal powers at the input of the nodes are approximately similar (Table 4.4) and as such a reliable signal transmission is possible, which is apparent in Figure 4.10. Furthermore, the threshold value of all DIG elements can be set to 0.004 a.u. (depicted in the AMP's plots of Figure 4.10 as dashed lines) and the signal be reconstructed correctly in digital domain.

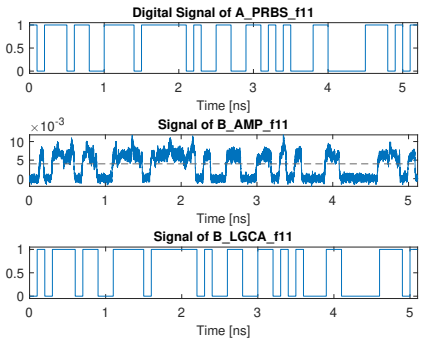

(a) ONI_A to ONI_B via f_1.

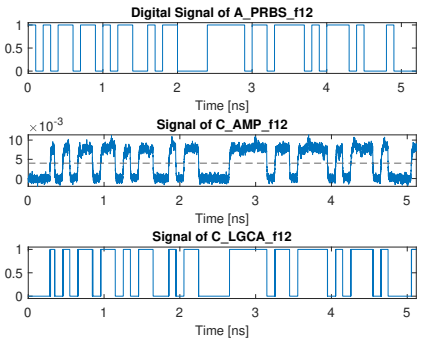

(b) ONI_A to ONI_C via f_2.

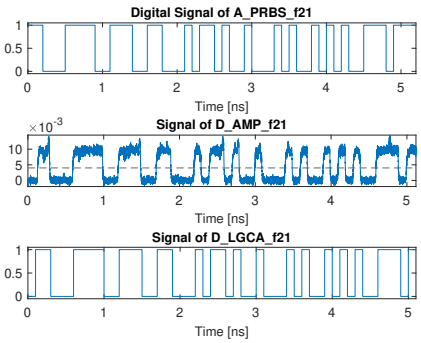

(c) ONI_A to ONI_D via f_1.

Figure 4.10.: Transmitted Signals (second configuration, setup 2).

	Signal Power	SNR
f_{11}	−4.01 dBm	13.43 dB
f_{12}	−4.96 dBm	14.30 dB
f_{21}	−4.90 dBm	15.54 dB

(a) ONI_A

	Signal Power	SNR
f_{11}	−4.87 dBm	15.41 dB
f_{21}	−3.18 dBm	16.55 dB
f_{22}	−5.13 dBm	14.14 dB

(b) ONI_B

	Signal Power	SNR
f_{11}	−3.46 dBm	15.09 dB
f_{12}	−4.01 dBm	15.05 dB
f_{21}	−4.84 dBm	15.22 dB

(c) ONI_C

	Signal Power	SNR
f_{11}	−6.58 dBm	14.76 dB
f_{21}	−3.71 dBm	14.48 dB
f_{22}	−4.28 dBm	15.47 dB

(d) ONI_D

Table 4.4.: Signal powers and SNRs (second configuration, setup 2).

Setup 3

With the parameters from [37], frequency f_1 can be set to 193.1 THz and frequency f_2 to 194.3 THz. An increased FSR of 2.54 THz allows a broader frequency separation, which is reflected in Figure 4.11.

The transmission behaviour is shown in Figure 4.12. As can be seen, in the presence of noise the laser power of 1 mW is not yet sufficient to ensure reliable reconstruction of the signal at the receiver. Here, signal reconstruction may be possible in the transmission from ONI_A to ONI_B (Figure 4.12a) and to ONI_D (Figure 4.12c), but no to safely in the transmission to ONI_C (Figure 4.12b).

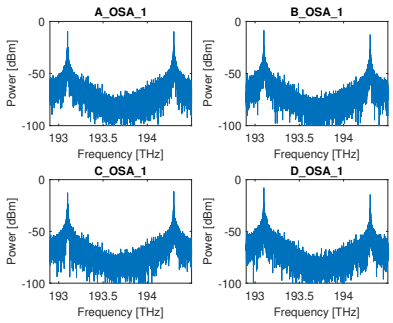

(a) Signals of the inner waveguide's OSAs.

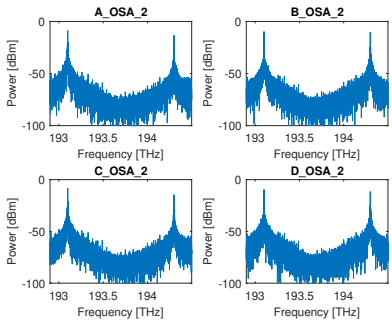

(b) Signals of the outer waveguide's OSAs.

Figure 4.11.: Signals recored by OSAs (second configuration, setup 3).

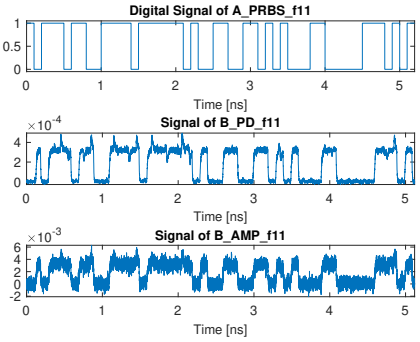

(a) ONI_A to ONI_B via f_1.

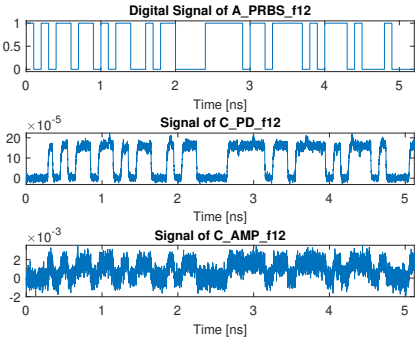

(b) ONI_A to ONI_C via f_2.

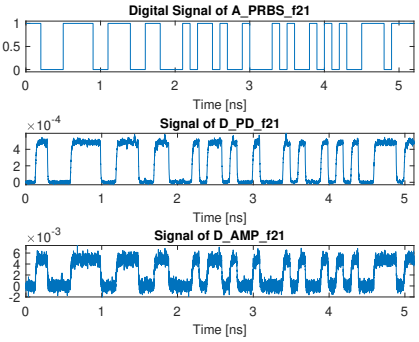

(c) ONI_A to ONI_D via f_1.

Figure 4.12.: Transmitted Signals (second configuration, setup 3).

This is also reflected in the signal powers and the SNRs, listed in Table 4.5; a signal power of approximately -12 dBM to -11 dBm for frequency f_2 (rows f_{12} and f_{22}) means a too low amplitude (10^{-5}) at the receiver. For this reason, the laser powers are to be adjusted in a further setup so that the signal powers listed in Table 4.5 are similar to the signal powers of setup 2 (Table 4.4).

	Signal Power	SNR
f_{11}	−6.08 dBm	15.29 dB
f_{12}	−11.85 dBm	14.32 dB
f_{21}	−7.83 dBm	15.45 dB

(a) ONI_A

	Signal Power	SNR
f_{11}	−7.84 dBm	15.39 dB
f_{21}	−6.14 dBm	16.68 dB
f_{22}	−12.03 dBm	14.28 dB

(b) ONI_B

	Signal Power	SNR
f_{11}	−6.43 dBm	15.31 dB
f_{12}	−10.92 dBm	15.16 dB
f_{21}	−7.79 dBm	15.56 dB

(c) ONI_C

	Signal Power	SNR
f_{11}	−9.48 dBm	14.94 dB
f_{21}	−6.63 dBm	14.79 dB
f_{22}	−11.19 dBm	15.58 dB

(d) ONI_D

Table 4.5.: Signal powers and SNRs (second configuration, setup 3).

Setup 4

In this setup, the laser powers were adjusted to 2 mW for frequency f_1 and to 5 mW for frequency f_2. As such the total laser power sums up to

$$P_{tot} = 8 * 2\,\text{mW} + 4 * 5\,\text{mW} = 36\,\text{mW} \tag{4.7}$$

The OSA's recorded spectra reflect the increased laser powers (Figure 4.13).

Due to the slight adjustment of laser powers, a reliable signal transmission is possible, which is indicated by the plotted transmission from ONI_A to the other nodes (Figure 4.14). All amplified signals have approximately the same amplitude (10^{-3}).

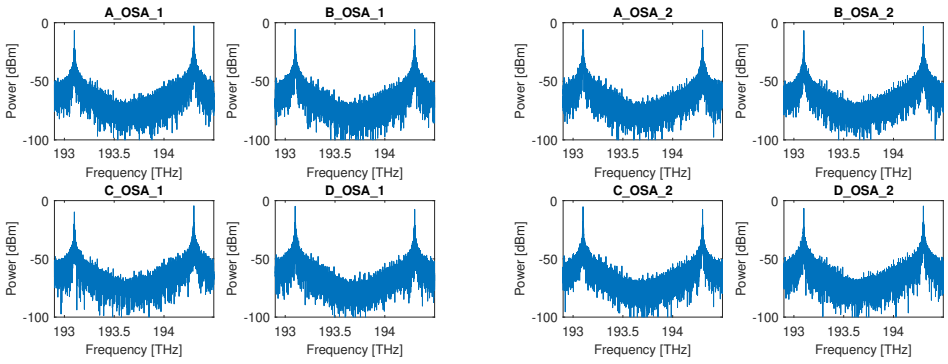

(a) Signals of the inner waveguide's OSAs. **(b)** Signals of the outer waveguide's OSAs.

Figure 4.13.: Signals recored by OSAs (second configuration, setup 4).

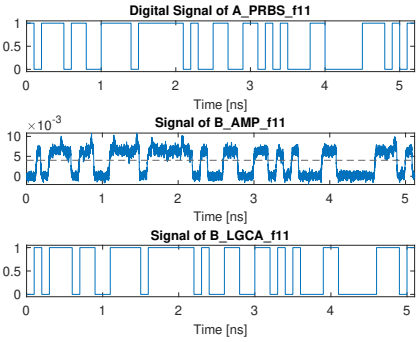

(a) ONI_A to ONI_B via f_1.

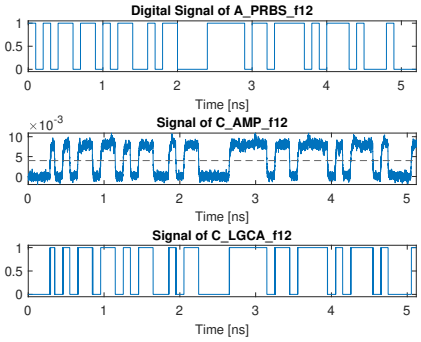

(b) ONI_A to ONI_C via f_2.

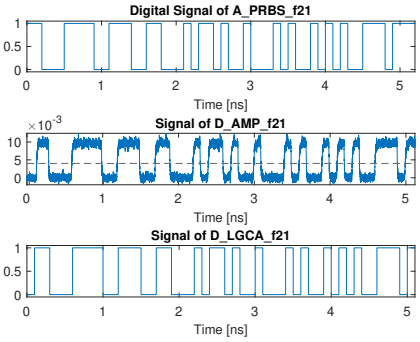

(c) ONI_A to ONI_D via f_1.

Figure 4.14.: Transmitted Signals (second configuration, setup 4.

The received signals all have an equal amplitude after amplification, because signal powers at the input of the nodes are similar (Table 4.6). As such, the threshold value of all DIG elements can be set to 0.004 a.u. (depicted in the AMP's plots of Figure 4.14 as dashed lines) and the signal be reconstructed correctly in digital domain.

Also for the second configuration the delay should be considered. The delay for short channels (via frequency f_1, e.g. ONI_A to ONI_B) is 0.1 ns, and 0.4 ns for mid-range channels (via frequency f_2, e.g. ONI_A to ONI_C).

	Signal Power	SNR
f_{11}	−3.07 dBm	15.30 dB
f_{12}	−4.86 dBm	14.32 dB
f_{21}	−4.82 dBm	15.45 dB

(a) ONI_A

	Signal Power	SNR
f_{11}	−4.83 dBm	15.40 dB
f_{21}	−3.13 dBm	16.68 dB
f_{22}	−5.04 dBm	14.28 dB

(b) ONI_B

	Signal Power	SNR
f_{11}	−3.42 dBm	15.31 dB
f_{12}	−3.93 dBm	15.16 dB
f_{21}	−4.78 dBm	15.57 dB

(c) ONI_C

	Signal Power	SNR
f_{11}	−6.47 dBm	14.94 dB
f_{21}	−3.62 dBm	14.79 dB
f_{22}	−4.20 dBm	15.59 dB

(d) ONI_D

Table 4.6.: Signal powers and SNRs (second configuration, setup 4).

4.0.3. Comparison

Finally, the two configurations are compared. For this, all relevant parameters are listed in Table 4.7. Setup 2 and 4 of the second configuration only differ slightly regarding the SNR; as such a comparison between these two setups is not required.

While the first configuration uses one ring waveguide, the second configuration two ring waveguides. However, at the cost of more area in the physical layout, the latter configuration only requires two wavelengths compared to seven wavelengths in the first configuration. As such, less losses in *pass through* mode of ORRs and crosstalk noise can be achieved. Further - as expected - the reduced WDM level is reflected in a reduced total laser power; laser powers add up to 272 mW in the first configuration and to 36 mW in the second one. In contrast, the average SNR of the first configuration is bigger than the second configuration. As stated above, the observed phenomenon eludes a comprehensive explanation. Finally, the maximum latency differentiates the two configurations. The lower maximum latency of the second configuration (0.4 ns) is possible, because the use of two ring waveguides avoids long-range channels.

Parameter	First Configuration	Second Configuration
SDM degree	1	2
WDM degree	7	2
Total laser power	272 mW	36 mW
Average SNR	17.28 dB	14.95 dB (15.23 dB)
Maximum delay	0.7 ns	0.4 ns

Table 4.7.: Comparison of the two configurations.

5. Conclusion

In this work, two configurations for a full functioning four-node ORNoC with full connectivity were simulated in Ansys Lumerical INTERCONNECT. By adjusting properties from [33] and [37], a functioning ORNoC was implemented and optimized.

The ORNoC is based on WDM, which allows for the simultaneous transmission of multiple optical signals at different wavelengths over a single waveguide. The wavelength dictates the destination. In both configurations a node is an ONI that comprises a receiving and transmitting side. The receiving side uses ORRs to direct light of a specific wavelength out of the waveguide torwards a PD, that detects light of this specific wavelength and generates an electrical signal based on the light's amplitude. Due to its weakness, the signal is amplified and converted into a digital signal using a DIG element, which models ADC conversion. On the transmitting side, a random electrical signal in not-return-to-zero line code is generated by a PRBS and an NRZ element and used as input to an ORM. The ORM modulates the amplitude of an optical signal (created by an OCL) based on the electrical signal and injects the modulated optical signal in the waveguide.

The first configuration physically connects the four nodes via one waveguide. Virtually, seven wavelengths are required to achieve full connectivity. Frequency f_1 is used for short channels, f_2 and f_3 for mid-range channels, and f_4, f_5, f_6 and f_7 for long-range channels. The configuration is favorable in terms of the number of waveguides.

The second configurations employs two waveguides. The optical signal progresses in clock-wise direction in the inner waveguide, and in counter clock-wise direction in the outer waveguide. As such, only two wavelengths are required for full connectivity. Frequency f_1 connects neighbouring nodes in both directions (short channels), while frequency f_2 provides the missing links (mid-range channels). Due to the lower number of wavelengths per waveguide, the configuration is characterized by an improved total laser power and lower maximum delay.

In future works, in order to obtain a more realistic model and more degrees of freedom for optimization, the PIC should be adapted and/or expanded. The first step would be to evaluate the current capabilities of PICs. From this, for example, state of the art properties of waveguides, ORRs and ORMs could be used for the simulations. Then, as explained in chapter 3, the ORM primitive element should be replaced by a combination of phase shifters, waveguides and couplers, the ORR

primitive element by a combination of waveguides and couplers. Because the ORR's and ORM's model descriptions lack a clear explanation of how the FSR is obtained (the theoretical formula does not match the results), the use of primitive elements to create an ORM and ORR compound may offer much more flexibility for optimization. Moreover, waveguides, whose length corresponds to the distance between two cores in a multi-chore architecture or two functional components in a SoC, can replace the 0-db attenuators at the interface between two nodes, making the model even more realistic.

Furthermore, for the configurations described above, properties were taken from related works. To obtain and optimize individual properties, simulations of individual components in a finite element analysis software such as COMSOL Multiphysics or related Lumerical simulators should be carried out. For instance, loss, group index, dispersion, and coupling coefficient from [37] were extracted from 2.5D FDTD simulations of the ring resonator waveguide and coupler in Lumerical MODE Solutions. Similar simulations could be performed with indivdual inputs and for all components.

In a long-term perspective, not only ORNoCs, but ONoCs architectures in general are a promising solution for global communication between a ever growing number of cores and or functional units on a chip. As such, the proposition of Moore's law could continue to prove correct.

Bibliography

[1] C. Leiserson *et al.*, "There's plenty of room at the Top: What will drive computer performance after Moore's law?" *Science*, vol. 368, Jun. 2020. DOI: 10.1126/science.aam9744.

[2] B. Bohnenstiehl *et al.*, "KiloCore: A 32-nm 1000-Processor Computational Array," *IEEE Journal of Solid-State Circuits*, vol. 52, no. 4, pp. 891–902, 2017. DOI: 10.1109/JSSC.2016.2638459.

[3] IEEE. "IRDS 2021 Edition - More Moore Whitepaper." (2021), [Online]. Available: https://irds.ieee.org/images/files/pdf/2016_MM.pdf (visited on 04/23/2024).

[4] IEEE. "International Roadmap for Devices and Systems." (2024), [Online]. Available: https://irds.ieee.org/ (visited on 04/23/2024).

[5] R. K. May. "More than Moore: the next steps for the semiconductor industry." (2023), [Online]. Available: https://blog.delmic.com/more-than-moore-the-next-steps-for-the-semiconductor-industry (visited on 04/23/2024).

[6] C. Sun *et al.*, "DSENT - A Tool Connecting Emerging Photonics with Electronics for Opto-Electronic Networks-on-Chip Modeling," in *2012 IEEE/ACM Sixth International Symposium on Networks-on-Chip*, 2012, pp. 201–210. DOI: 10.1109/NOCS.2012.31.

[7] S. Le Beux *et al.*, "Optical Ring Network-on-Chip (ORNoC): Architecture and design methodology," in *2011 Design, Automation Test in Europe*, 2011, pp. 1–6. DOI: 10.1109/DATE.2011.5763134.

[8] V. Adler and E. Friedman, "Repeater design to reduce delay and power in resistive interconnect," *IEEE Transactions on Circuits and Systems II: Analog and Digital Signal Processing*, vol. 45, no. 5, pp. 607–616, 1998. DOI: 10.1109/82.673643.

[9] W. Green *et al.*, "Silicon photonic wire circuits for on-chip optical interconnects," vol. 6883, Feb. 2008. DOI: 10.1117/12.767340.

[10] S. Werner, J. Navaridas, and M. Luján, "A Survey on Optical Network-on-Chip Architectures," *ACM Comput. Surv.*, vol. 50, no. 6, Dec. 2017. DOI: https://doi.org/10.1145/3131346.

[11] H. Ishio, J. Minowa, and K. Nosu, "Review and status of wavelength-division-multiplexing technology and its application," *Journal of Lightwave Technology*, vol. 2, no. 4, pp. 448–463, 1984. DOI: 10.1109/JLT.1984.1073653.

[12] M. Ortín-Obón *et al.*, "Contrasting Laser Power Requirements of Wavelength-Routed Optical NoC Topologies Subject to the Floorplanning, Placement, and Routing Constraints of a 3-D-Stacked System," *IEEE Transactions on Very Large Scale Integration (VLSI) Systems*, vol. 25, no. 7, pp. 2081–2094, 2017. DOI: 10.1109/TVLSI.2017.2677779.

[13] R. Osgood jr. and X. Meng, *Principles of Photonic Integrated Circuits. Materials, Device Physics, Guided Wave Design*. Springer Cham, 2021. DOI: 10.1007/978-3-030-65193-0.

[14] C. R. Pollock and M. Lipson, *Integrated Photonics*. New York, NY: Springer New York, 2003. DOI: 10.1007/978-1-4757-5522-0.

[15] W. Bogaerts *et al.*, "Silicon microring resonators," *Laser & Photonics Reviews*, vol. 6, no. 1, pp. 47–73, 2012. DOI: 10.1002/lpor.201100017.

[16] M. J. R. Heck and J. E. Bowers, "Energy Efficient and Energy Proportional Optical Interconnects for Multi-Core Processors: Driving the Need for On-Chip Sources," *IEEE Journal of Selected Topics in Quantum Electronics*, vol. 20, no. 4, pp. 332–343, 2014. DOI: 10.1109/JSTQE.2013.2293271.

[17] COMSOL. "COMSOL Multiphysics." (2024), [Online]. Available: https://www.comsol.com (visited on 04/02/2024).

[18] Synopsis. "Synoptis OptSim." (2024), [Online]. Available: https://www.synopsys.com/photonic-solutions/optsim/single-mode-network.html (visited on 04/02/2024).

[19] Ansys. "Ansys Lumerical INTERCONNECT." (2024), [Online]. Available: https://www.ansys.com/products/optics/interconnect (visited on 04/02/2024).

[20] Ansys. "Categorical list of INTERCONNECT Elements." (2024), [Online]. Available: https://optics.ansys.com/hc/en-us/articles/360036106954-Categorical-list-of-INTERCONNECT-Elements (visited on 04/02/2024).

[21] Ansys. "PRBS Generator (PRBS) - INTERCONNECT Element." (2024), [Online]. Available: https://optics.ansys.com/hc/en-us/articles/360036618013-PRBS-Generator-PRBS-INTERCONNECT-Element (visited on 04/02/2024).

[22] Ansys. "Data Recovery (DATA) - INTERCONNECT Element." (2024), [Online]. Available: https://optics.ansys.com/hc/en-us/articles/360036108854-Data-Recovery-DATA-INTERCONNECT-Element (visited on 04/02/2024).

[23] Ansys. "NRZ Pulse Generator (NRZ) - INTERCONNECT Element." (2024), [Online]. Available: https://optics.ansys.com/hc/en-us/articles/360036618053-NRZ-Pulse-Generator-NRZ-INTERCONNECT-Element (visited on 04/02/2024).

[24] Ansys. "CW Laser (CWL) - INTERCONNECT Element." (2024), [Online]. Available: https://optics.ansys.com/hc/en-us/articles/360036618173-CW-Laser-CWL-INTERCONNECT-Element (visited on 04/02/2024).

[25] Ansys. "Electrical Amplifier (AMP) - INTERCONNECT Element." (2024), [Online]. Available: https://optics.ansys.com/hc/en-us/articles/360036108254-Electrical-Amplifier-AMP-INTERCONNECT-Element (visited on 04/02/2024).

[26] Ansys. "Oscilloscope (OSC) - INTERCONNECT Element." (2024), [Online]. Available: https://optics.ansys.com/hc/en-us/articles/360036107054-Oscilloscope-OSC-INTERCONNECT-Element (visited on 04/02/2024).

[27] Ansys. "Logic Analyzer (LGCA) - INTERCONNECT Element." (2024), [Online]. Available: https://optics.ansys.com/hc/en-us/articles/360036107034-Logic-Analyzer-LGCA-INTERCONNECT-Element (visited on 04/02/2024).

[28] Ansys. "Optical Spectrum Analyzer (OSA) - INTERCONNECT Element." (2024), [Online]. Available: https://optics.ansys.com/hc/en-us/articles/360036617913-Optical-Spectrum-Analyzer-OSA-INTERCONNECT-Element (visited on 04/02/2024).

[29] Ansys. "Optical Channel Analyzer (OCN) - INTERCONNECT Element." (2024), [Online]. Available: https://optics.ansys.com/hc/en-us/articles/360036107174-Optical-Channel-Analyzer-OCN-INTERCONNECT-Element (visited on 04/02/2024).

[30] Ansys. "Optical Network Analyzer (ONA) - INTERCONNECT Element." (2024), [Online]. Available: https://optics.ansys.com/hc/en-us/articles/360036617973-Optical-Network-Analyzer-ONA-INTERCONNECT-Element (visited on 04/02/2024).

[31] Ansys. "INTERCONNECT: Enabling time and frequency domain simulation of photonic integrated circuits with microring modulators." (2024), [Online]. Available: https://www.lumerical.com/learn/whitepapers/interconnect-enabling-time-and-frequency-domain-simulation-of-photonic-integrated-circuits-with-microring-modulators/ (visited on 04/02/2024).

[32] Ansys. "Optical Ring Modulator (RING) - INTERCONNECT Element." (2024), [Online]. Available: https://optics.ansys.com/hc/en-us/articles/360036107694-Optical-Ring-Modulator-RING-INTERCONNECT-Element (visited on 04/02/2024).

[33] Ansys. "Wavelength division multiplexing." (2024), [Online]. Available: https://optics.ansys.com/hc/en-us/articles/360042322774-Wavelength-division-multiplexing (visited on 04/02/2024).

[34] Ansys. "Ring resonator using INTERCONNECT primitive elements." (2024), [Online]. Available: https://optics.ansys.com/hc/en-us/articles/360042323794-Ring-resonator-using-INTERCONNECT-primitive-elements (visited on 04/02/2024).

[35] Ansys. "Double Bus Ring Resonator (RES) - INTERCONNECT Element." (2024), [Online]. Available: https://optics.ansys.com/hc/en-us/articles/360036618833-Double-Bus-Ring-Resonator-RING-INTERCONNECT-Element,%20CONNECT%20TO%20ABOVE (visited on 04/02/2024).

[36] Ansys. "Optical Attenuator (ATT) - INTERCONNECT Element." (2024), [Online]. Available: https://optics.ansys.com/hc/en-us/articles/360036618373-Optical-Attenuator-ATT-INTERCONNECT-Element (visited on 04/02/2024).

[37] C. Chen, M. N., and V. Stojanovic. "An Optical Wavelength-Division Multiplexed Communication Link." (2017), [Online]. Available: https://e3s-center.berkeley.edu/wp-content/uploads/2017/07/Chen_Cecilia_Poster_v3.pdf (visited on 04/23/2024).

A. Properties

A.1. First Configuration

A.1.1. Setup 1

Standard properties were used for the simulator options, except the bitrate. It was set to 10 Gbit/s.

f_1	f_2	f_3	f_4	f_5	f_6	f_7
193.065	193.265	193.465	193.665	193.865	194.065	194.265

Table A.1.: Frequencies of the Optical Ring Modulators and Lasers (in THz).

f_1	f_2	f_3	f_4	f_5	f_6	f_7
193.075	193.275	193.475	193.675	193.875	194.075	194.275

Table A.2.: Frequencies of other elements (in THz).

Category	Property	Value
Standard	frequency	...
	length	6×10^{-5} m
Waveguide	loss	7 dB/m
	group index	4.42
	coupling efficient 1	0.1
	coupling efficient 2	0.1
Numerical/Digital Filter	time variant digital filter	interpolate

Table A.3.: Optical Ring Modulators

Category	Property	Value
Standard	frequency	...
	length	6×10^{-5} m
Waveguide/Mode 1 & 2	group index 1 & 2	4.42
Waveguide/Mode 1 & 2/Coupler	coupling efficient 1 1 & 2	0.1
	coupling efficient 2 1 & 2	0.1

Table A.4.: Optical Ring Resonators

Category	Property	Value
Standard	frequency	...
	power	0.001 W

(a) Lasers

Category	Property	Value
Standard	gain	20 dB
	noise parameter	disable

(b) (Electrical) Amplifier

Category	Property	Value
Standard	frequency	...
Numerical	enable thermal noise	false
	enable shot noise	false

(c) Photodetectors

Category	Property	Value
Standard	amplitude	0.4 a.u
	bias	0.6 a.u.

(d) Non-Return-To-Zero Elements

Table A.5.: Other components

A.1.2. Setup 2

Standard properties were used for the simulator options, except the bitrate. It was set to 10 Gbit/s.

f_1	f_2	f_3	f_4	f_5	f_6	f_7
193.1	193.4	193.7	194	194.3	194.6	194.9

Table A.6.: Frequencies of all elements (in THz).

Category	Property	Value
Standard	frequency	...
	length	3×10^{-5} m
Waveguide	loss	3.45578 dB/m
	group index	3.93544
	dispersion	-0.0015015 s/m/m
	coupling efficient 1	0.046
	coupling efficient 2	0.046
Numerical/Digital Filter	time variant digital filter	interpolate

Table A.7.: Optical Ring Modulators

Category	Property	Value
Standard	frequency	...
	length	3×10^{-5} m
Waveguide/Mode 1 & 2	loss 1 & 2	3.45578 dB/m
	group index 1 & 2	3.93544
	group index 1 & 2	-0.0015015 s/m/m
Waveguide/Mode 1 & 2/Coupler	coupling efficient 1 1 & 2	0.046
	coupling efficient 2 1 & 2	0.046

Table A.8.: Optical Ring Resonators

input (a.u.)	output (a.u.)
0	0
0.001	1

(a) Short channels

input (a.u.)	output (a.u.)
0	0
0.0003	1

(b) Mid-range channels

input (a.u.)	output (a.u.)
0	0
0.0001	1

(c) Long-range channels

Table A.9.: Threshold Table of DIG elements

Category	Property	Value
Standard	frequency	...
	power	0.001 W

(a) Lasers

Category	Property	Value
Standard	gain	20 dB
	noise parameter	disable

(b) (Electrical) Amplifier

Category	Property	Value
Standard	frequency	...
Numerical	enable thermal noise	false
	enable shot noise	false

(c) Photodetectors

Category	Property	Value
Standard	amplitude	0.4 a.u
	bias	0.6 a.u.

(d) Non-Return-To-Zero elements

Table A.10.: Other components

A.1.3. Setup 3

Standard properties were used for the simulator options, except the bitrate. It was set to 10 Gbit/s.

f_1	f_2	f_3	f_4	f_5	f_6	f_7
193.1	193.4	193.7	194	194.3	194.6	194.9

Table A.11.: Frequencies of all elements (in THz).

Category	Property	Value
Standard	frequency	...
	length	3×10^{-5} m
Waveguide	loss	3.45578 dB/m
	group index	3.93544
	dispersion	-0.0015015 s/m/m
	coupling efficient 1	0.046
	coupling efficient 2	0.046
Numerical/Digital Filter	time variant digital filter	interpolate

Table A.12.: Optical Ring Modulators

Category	Property	Value
Standard	frequency	...
	length	3×10^{-5} m
Waveguide/Mode 1 & 2	loss 1 & 2	3.45578 dB/m
	group index 1 & 2	3.93544
	group index 1 & 2	-0.0015015 s/m/m
Waveguide/Mode 1 & 2/Coupler	coupling efficient 1 1 & 2	0.046
	coupling efficient 2 1 & 2	0.046

Table A.13.: Optical Ring Resonators

Category	Property	Value
Standard	frequency	f_1
	power	0.003 W

(a) Short channels

Category	Property	Value
Standard	frequency	f_2, f_3
	power	0.015 W

(b) Mid-range channels

Category	Property	Value
Standard	frequency	f_4, f_5, f_6, f_7
	power	0.05 W

(c) Long-range channels

Table A.14.: Laser properties

input (a.u.)	output (a.u.)
0	0
0.004	1

Table A.15.: Threshold Table of all DIG elements

Category	Property	Value
Standard	amplitude	0.4 a.u
	bias	0.6 a.u.

(a) Non-Return-To-Zero elements

Category	Property	Value
Standard	gain	20 dB
	noise parameter	noise figure

(b) (Electrical) Amplifier

Category	Property	Value
Standard	frequency	...
Numerical	enable thermal noise	true
	enable shot noise	true

(c) Photodetectors

Table A.16.: Other components

A.2. Second Configuration

A.2.1. Setup 1

Standard properties were used for the simulator options, except the bitrate. It was set to 10 Gbit/s.

f_1	f_2
193.075	193.675

Table A.17.: Frequencies of all elements (in THz).

Category	Property	Value
Standard	frequency	...
	length	6×10^{-5} m
Waveguide	loss	7 dB/m
	group index	4.42
	coupling efficient 1	0.1
	coupling efficient 2	0.1
Numerical/Digital Filter	time variant digital filter	interpolate

Table A.18.: Optical Ring Modulators

Category	Property	Value
Standard	frequency	...
	length	6×10^{-5} m
Waveguide/Mode 1 & 2	group index 1 & 2	4.42
Waveguide/Mode 1 & 2/Coupler	coupling efficient 1 1 & 2	0.1
	coupling efficient 2 1 & 2	0.1

Table A.19.: Optical Ring Resonators

Category	Property	Value
Standard	frequency	...
	power	0.001 W

(a) Lasers

Category	Property	Value
Standard	gain	20 dB
	noise parameter	noise figure

(b) (Electrical) Amplifier

Category	Property	Value
Numerical	enable thermal noise	true
	enable shot noise	true

(c) Photodetectors

Category	Property	Value
Standard	amplitude	0.4 a.u
	bias	0.6 a.u.

(d) Non-Return-To-Zero elements

Table A.20.: Other components

A.2.2. Setup 2

Standard properties were used for the simulator options, except the bitrate. It was set to 10 Gbit/s.

f_1	f_2
193.075	193.675

Table A.21.: Frequencies of all elements (in THz).

Category	Property	Value
Standard	frequency	...
	length	6×10^{-5} m
Waveguide	loss	7 dB/m
	group index	4.42
	coupling efficient 1	0.1
	coupling efficient 2	0.1
Numerical/Digital Filter	time variant digital filter	interpolate

Table A.22.: Optical Ring Modulators

Category	Property	Value
Standard	frequency	...
	length	6×10^{-5} m
Waveguide/Mode 1 & 2	group index 1 & 2	4.42
Waveguide/Mode 1 & 2/Coupler	coupling efficient 1 1 & 2	0.1
	coupling efficient 2 1 & 2	0.1

Table A.23.: Optical Ring Resonators

Category	Property	Value
Standard	frequency	f_1
	power	0.002 W

(a) Short channels

Category	Property	Value
Standard	frequency	f_2, f_3
	power	0.005 W

(b) Mid-range channels

Table A.24.: Laser properties

input (a.u.)	output (a.u.)
0	0
0.004	1

Table A.25.: Threshold Table of all DIG elements

A.2.3. Setup 3

Standard properties were used for the simulator options, except the bitrate. It was set to 10 Gbit/s.

f_1	f_2
193.1	194.3

Table A.26.: Frequencies of all elements (in THz).

Category	Property	Value
Standard	frequency	...
	length	3×10^{-5} m
Waveguide	loss	3.45578 dB/m
	group index	3.93544
	dispersion	-0.0015015 s/m/m
	coupling efficient 1	0.046
	coupling efficient 2	0.046
Numerical/Digital Filter	time variant digital filter	interpolate

Table A.27.: Optical Ring Modulator

Category	Property	Value
Standard	frequency	...
	length	3×10^{-5} m
Waveguide/Mode 1 & 2	loss 1 & 2	3.45578 dB/m
	group index 1 & 2	3.93544
	group index 1 & 2	-0.0015015 s/m/m
Waveguide/Mode 1 & 2/Coupler	coupling efficient 1 1 & 2	0.046
	coupling efficient 2 1 & 2	0.046

Table A.28.: Optical Ring Resonator

Category	Property	Value
Standard	frequency	...
	power	0.001 W

(a) Lasers

Category	Property	Value
Standard	amplitude	0.4 a.u
	bias	0.6 a.u.

(b) Non-Return-To-Zero Elements

Category	Property	Value
Numerical	enable thermal noise	true
	enable shot noise	true

(c) Photodetectors

Category	Property	Value
Standard	gain	20 dB
	noise parameter	noise figure

(d) (Electrical) Amplifier

Table A.29.: Other components

A.2.4. Setup 4

Standard properties were used for the simulator options, except the bitrate. It was set to 10 Gbit/s.

f_1	f_2
193.1	194.3

Table A.30.: Frequencies of all elements (in THz).

Category	Property	Value
Standard	frequency	...
	length	3×10^{-5} m
Waveguide	loss	3.45578 dB/m
	group index	3.93544
	dispersion	-0.0015015 s/m/m
	coupling efficient 1	0.046
	coupling efficient 2	0.046
Numerical/Digital Filter	time variant digital filter	interpolate

Table A.31.: Optical Ring Modulator

Category	Property	Value
Standard	frequency	...
	length	3×10^{-5} m
Waveguide/Mode 1 & 2	loss 1 & 2	3.45578 dB/m
	group index 1 & 2	3.93544
	group index 1 & 2	-0.0015015 s/m/m
Waveguide/Mode 1 & 2/Coupler	coupling efficient 1 1 & 2	0.046
	coupling efficient 2 1 & 2	0.046

Table A.32.: Optical Ring Resonator

Category	Property	Value
Standard	frequency	f_1
	power	0.002 W

(a) Short channels

Category	Property	Value
Standard	frequency	f_2, f_3
	power	0.005 W

(b) Mid-range channels

Table A.33.: Laser properties

input (a.u.)	output (a.u.)
0	0
0.004	1

Table A.34.: Threshold Table of all DIG element

Category	Property	Value
Standard	amplitude	0.4 a.u
	bias	0.6 a.u.

(a) Non-Return-To-Zero Elements

Category	Property	Value
Numerical	enable thermal noise	true
	enable shot noise	true

(b) Photodetectors

Category	Property	Value
Standard	gain	20 dB
	noise parameter	noise figure

(c) (Electrical) Amplifier

Table A.35.: Other components